GEORGIA DOT RESEARCH PROJECT RP16-24

FINAL REPORT

MECHANICAL INTEGRITY AND SUSTAINABILITY OF PRE-STRESSED CONCRETE BRIDGE GIRDERS REPAIRED BY EPOXY INJECTION – PHASE 1

OFFICE OF RESEARCH
15 KENNEDY DRIVE
FOREST PARK, GA 30297-2534

TECHNICAL REPORT STANDARD TITLE PAGE

1.Report No.: FHWA-GA-17-1624	2. Government Accession No.:	3. Recipient's Catalog No.:
4. Title and Subtitle: Mechanical Integrity and Sustainability of Pre-Stressed Concrete Bridge Girders Repaired by Epoxy Injection – Phase 1	5. Report Date: February 2017	
	6. Performing Organization Code:	
7. Author(s): Dr. Arson Chloe, Ph.D. Mr. Koochul Ji	8. Performing Organ. Report No.: 16-24	
9. Performing Organization Name and Address: Georgia Institute of Technology School of Civil & Environmental Engineering 790 Atlantic Drive Atlanta, GA 30318	10. Work Unit No.:	
	11. Contract or Grant No.: 0013731	
12. Sponsoring Agency Name and Address: Georgia Department of Transportation Office of Research 15 Kennedy Drive Forest Park, GA 30297-2534	13. Type of Report and Period Covered: Final: October 2016 – January 2017	
	14. Sponsoring Agency Code:	

15. Supplementary Notes:

16. Abstract:
The ultimate goal of this project is to assess the mechanical integrity and sustainability of pre-stressed concrete beams during the entire life cycle of the built infrastructure, which includes crack propagation, crack reparation, repaired crack aging with possible re-opening. In Phase I, the research objectives are to: (1) Explain in which conditions the strength of cracked concrete can be recovered by epoxy injection; (2) Design the injection method for optimal mechanical performance. Since the mid-point review, the main achievements in this project period have been: the design of FEM models comprising concrete elements and pre-stressed steel bar reinforcements for four types of girders, used in Tennessee, Washington State, Virginia and Florida; the simulation of load tests reported in the literature for these four girders, with elastic concrete; the modeling of four types of cracks described in the PCI manual; the simulation of the load test for the four types of girders, for the four types of damage; the assessment of the effect of initial damage on the stress distribution and on the deflection of the girders; a literature review on the Cohesive Zone Models that can be used to predict not only the mechanical damage, but also the geometric discontinuities induced by fracture propagation in concrete.

17. Key Words: Epoxy injection, Pre-stressed concrete girder, Concrete crack	18. Distribution Statement:		
19. Security Classification (of this report): Unclassified	20. Security Classification (of this page): Unclassified	21. Number of Pages: 89	22. Price:

Form DOT 1700.7 (8-69)

GDOT Research Project No. RP16-24

Final Report

Mechanical Integrity and Sustainability of Pre-Stressed Concrete Bridge Girders Repaired by Epoxy Injection – Phase 1

By

Chloe Arson, Ph.D.
Principal Investigator
Koochul Ji
Research Assistant

Georgia Institute of Technology

Contract with

Georgia Department of Transportation

In cooperation with

U.S. Department of Transportation
Federal Highway Administration

Feb 2017

LIST OF TABLES

LIST OF FIGURES

EXECUTIVE SUMMARY

At present, there is a need to assess the mechanical integrity and sustainability of pre-stressed concrete beams during the entire life cycle of the built infrastructure. According to the NCHRP (Tadros et al., 2010), "further research to develop finite element modeling of the end zone of pre-tensioned members should be of value in optimizing the bursting reinforcement". The ultimate goal of this project is to assess the mechanical integrity and sustainability of pre-stressed concrete beams during the entire life cycle of the built infrastructure, which includes crack propagation, crack reparation, repaired crack aging with possible re-opening. In Phase I, the research objectives are to: (1) Explain in which conditions the strength of cracked concrete can be recovered by epoxy injection; (2) Design the injection method for optimal mechanical performance.

We explained how epoxy is used to repair cracked concrete and we summarized the governing equations of epoxy rheological models. We presented the governing equations of the Differential Stress-Induced Damage model (DSID), a Continuum Damage Mechanics model that allows predicting the propagation of cracks in three directions, according to net tension and compression criteria. The damage variable is similar to a crack density tensor. We calibrated and validated the DSID model to match stress/strain curves obtained during concrete triaxial compression tests reported in the literature. We performed DSID model sensitivity analyses with a MATLAB code. Simulations were done at the material point for tensile and compressive stress paths. Results show that cracks propagate in planes perpendicular to the maximum deviatoric stress, and that stiffness decreases in the directions in which damage increases.

Simulations confirm that mechanical effects of cracks before and after reparation can be modeled by high and low damage.

We designed a Finite Element model of bridge deck with ABAQUS software. The model includes the steel-reinforced concrete deck and the pre-stressed steel-reinforced girders. We applied the static loads recommended in the design standards to predict the displacement and stress fields in the structure. Concrete was first considered elastic. Simulation results highlight the high stress concentrations at the ends of the girders and at the contact between the girders and the rubber pads lying at the top of the supporting columns. Then the FEM model was modified to account for crack propagation in the concrete. The DSID model was assigned to the concrete elements located in the girder subject to maximal stress (further away from the center of the deck). Static service loads were simulated. Results highlight the capability of the model to predict the initiation and orientation of the damage in the form of vertical cracks close to the interface between the concrete and the rubber pads. Loading tests were simulated with initial vertical damage (i.e. horizontal cracks) in order to assess the effect of longitudinal cracks due to pre-stress relaxation on the deflection and internal stresses of girders. Bridge simulations were repeated with initial damage in the end zone of the most highly stressed girder in the deck. Damage configurations corresponded to typical crack patterns listed in the PCI bridge repair guidelines. In general, lower stress and higher deflections were found for higher initial damage.

Load tests performed by other researchers on full-scale girders used in Tennessee, Washington State, Virginia and Florida were simulated, with and without initial damage. The FEM girder models accounted for the differences in the design of the prestressed

steel reinforcements. Initial damage values were chosen so as to represent four typical crack patterns described in the PCI manual, including: vertical cracks, horizontal cracks, diagonal cracks and cracks on the bottom flange. Simulation results did not indicate any significant impact of initial damage on stress distributions for the tests simulated. The effect of initial cracks on deflection was minimal; increased displacements were only noted in the area close to the point of application of the clamping force. The most noticeable effects on deflection were obtained for vertical and diagonal cracks. Simulation results show that initial damage in the end zone does not affect the mechanical response of the girder during the vertical load test, and that epoxy reparation is needed only to prevent steel corrosion.

Further analyses are needed to check the response of girders under a variety of stress paths including cyclic loading, and to calibrate the phenomenological damage variable against actual crack densities. In order to predict the geometry of cracks and not only their average effect on stiffness, we will use a Cohesive Zone Model (CZM) to represent crack patterns in the end zone. We presented a literature review of CZM, which can be coupled with the DSID model in order to predict the simultaneous propagation of cracks and their damage zone around the tip. The CZM provides an explicit geometric representation of cracks, which will allow determining the range of crack orientations that need to be considered for potential injection, the critical density of cracks in this range of orientations, the fraction of crack volume that needs to be filled with epoxy. We will examine several design criteria, including allowable girder deflection, allowable concrete stresses and strains, and optimal concrete strength in compression and shear. We will check whether PCI reparation recommendations are conservative or not.

ACKNOWLEDGMENTS

1. INTRODUCTION

The first pre-stressed concrete bridge constructed in the United States is the Walnut Lane Memorial Bridge (Philadelphia, Pennsylvania). It was built in 1951. Now, pre-stressed concrete girders are widely used in the United States for bridge construction. During pre-stress transfer, beams tend to bend upwards, which opens longitudinal cracks along the horizontal axis, especially at the end of the girders (Fig. 1-2). The mechanical integrity and reparation techniques of pre-stressed concrete girders thus raised particular interest in civil engineering research.
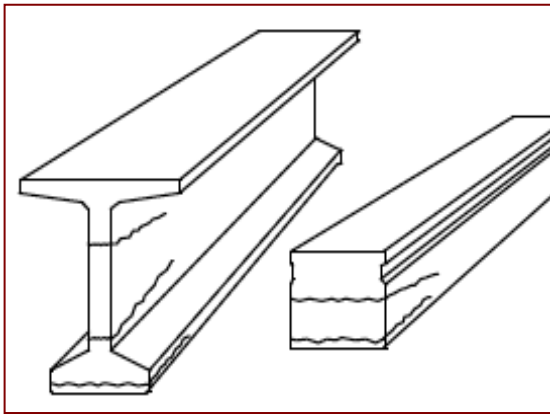
Figure 1: Expected geometry of longitudinal cracks in pre-stressed concrete bridge girders (PCI, 2001)

Figure 2: Longitudinal cracks due to pre-stress transfer in a 42-ft long, 45-in high Bulb-T girder (Tadros et al., 2010)

The main remediation techniques that are used to avert cracks are: Progressive pre-stress transfer (by pressing a hydraulic piston instead of flame cutting); Balanced pre-stress transfer (by cutting steel cables from both sides and from uniformly distributed locations of the cross section); Additional reinforcements (e.g., strands); Partial de-

bonding of strands (Kahl, 2011). The NCHRP has proposed the following remediation techniques for precast/pre-stressed concrete girders (Tadros et al., 2010):

- If the longitudinal cracks are less than 0.012 in. wide the girder is considered acceptable.

- For cracks between 0.012 in. and 0.025 in., grouting of cementitious packing materials is applied.

- When longitudinal cracks are between 0.025 in. and 0.050 in. wide, the longitudinal cracks are repaired by epoxy injection.

- If the cracks are wider than 0.05 in., the cracked pre-stressed girder should be replaced by a new pre-stressed concrete girder.

The Precast/Prestressed Concrete Institute (PCI) issued recommendations to accept, repair or reject girders, depending on the location, orientation, length and width of the cracks (PCI, 2012). Detailed reparation procedures are provided for eleven types of defects.

In the previous studies presented by the NCHRP (Tadros et al., 2010), the effects of longitudinal cracks on the mechanical performance of the girders were investigated by subjecting strip-shaped portions of cracked girders to mechanical testing (Fig.3). The experimental results show that longitudinal cracks could potentially cause corrosion but did not affect significantly the mechanical integrity and sustainability of the girder. Furthermore, when girders undergo vertical dead loads, the longitudinal cracks tend to close by compression. Consequently, epoxy injection was primarily recommended to seal the cracks and avoid water absorption, corrosion and steel concrete de-bonding – not for mechanical recovery of concrete properties. Other experimental studies (Issa and Debs,

2007) showed that 50% of the lost concrete strength could be recovered by epoxy injection. Epoxy injection can increase the fatigue resistance of cracked concrete, but the mechanical performance of repaired concrete decreases as temperature increases (Shin et al., 2011). Repaired pre-stressed concrete girders present a more brittle behavior than intact or corroded beams (Okada et al., 1988). Therefore, a detailed study of repaired concrete with epoxy injection is needed to verify the mechanical integrity and sustainability of pre-stressed concrete bridge girders repaired by epoxy injection.

| a. Bottom flange completely cut from the specimen. | b. Strip specimen tested between two bearing plates. | c. Strip specimen after testing. |

Figure 3: Mechanical tests performed on strip-shaped portions of cracked girders (Tadros et al., 2010).

1.1 PURPOSE OF THE STUDY

In 2008, 30% of the $60 billion federal transportation funds were used to build new roads or add capacity to existing roads, and 13% to repair bridges. More than 11% of the nation's roughly 600,000 highway bridges are classified as "structurally deficient," according to the Federal Highway Administration (FHWA). In 2010, 200,000 highway bridges had exceeded their expected lifespan of 50 years. "At the current rates of aging

and replacement, almost half of the nation's bridges will require major structural investments within the next 15 years" (T4america.org, 11/11/2015). In this context, it is crucial to assess the actual mechanical integrity of cracked structural components in bridges. The goal of this research is to optimize the use of epoxy injection to repair pre-stressed girders that contain a variety of crack patterns.

Current AASHTO recommendations for the injection of epoxy in longitudinal cracks are based on the extrapolation of experimental strength tests performed on a small number (less than 100) repaired structural members, in the short-term. This project aims to understand the mechanisms that govern crack propagation in pre-stressed girders, examine the mechanical integrity of cracked girders before and after epoxy injection, predict the evolution of mechanical damage upon cracking and reparation, and assess the sustainability of pre-stressed concrete bridge girders. Given the costs of beam replacement, best practices in mechanical damage diagnosis and epoxy injection could offer a highly cost-effective solution for bridge maintenance.

A damage model will be used to predict the mechanical performance of repaired concrete, which will allow simulating the life cycle of actual girders with the Finite Element Method. Sensitivity analyses will be conducted to understand the influence of mechanical loading, crack pattern, and crack filling over time, assuming a variety of loading conditions. The numerical analyses will support recommendations on when, where and how to practice epoxy injection so as to increase the expected lifespan of pre-stressed concrete bridge girders. In phase I, we propose a continuum-based approach to model the mechanical response of concrete, prestressed girders and bridge decks. We model girders with initial crack configurations similar to those listed in the PCI manual

and we simulate load tests to assess the influence of the cracks on the deflection and stress distribution in the girders.

1.2 REPORT ORGANIZATION

The project report is organized as follows:

- Section 1 gives a brief introduction of the project, explains the purpose of the study and presents the organization of the report.

- Section 2 provides a literature review of the behavior and characteristics of repaired concrete by epoxy resins.

- Section 3 summarizes the concrete properties of interest in this study, and explains the damage model used to represent cracks in the girders - the Differential Stresses Induced Damage (DSID) Model. This section also presents the method employed in this study to calibrate the DSID model against experimental results reported in the literature. Parametric studies on the mechanical behavior of damaged concrete are also reported.

- Section 4 presents a Finite Element model of bridge deck including the slab, the girders and the rubber pads. Static loads were simulated, for elastic and damageable concrete, with and without initial damage. Initial damage configurations were chosen to represent end zone crack patterns listed by the PCI in the girder that is subjected to the highest stresses.

- In Section 5, load tests performed at full scale on four different types of girders are simulated, with and without damage. Initial damage configurations were chosen to represent end zone crack patterns listed by the PCI.

- Section 6 presents the main principles of Cohesive Zone Models, which will be used in future studies to improve the representation of end zone crack patterns.

- Section 7 describes epoxy properties, and presents the linear and nonlinear epoxy resins models that are used in civil engineering. The governing equations of the non-linear viscoelastic model are presented in detail.

- Section 8 presents the main conclusions of phase I of this project.

2. LITERATURE REVIEW ON EPOXY-BASED REPARATION

Cracks in pre-stressed concrete may jeopardize the lifespan and structural sustainability of bridges. Cracks can initiate and propagate due to a variety of reasons including pre-stress girder fabrication, cyclic loading, static overload, temperature changes and chemical attacks. Concrete reparation by epoxy injection is widely used in the U.S. In order to validate the stability and mechanical integrity of resin-based reparation, experimental studies were conducted by I.A. Basunbul et al (1990), Issa and Debs (2007) and P. Duarte et al (2014). In the study by Issa and Debs, 15 concrete cubes (6 damaged concrete cubes without resin, 6 damaged concrete cubes repaired with epoxy resins, and 3 intact concrete cubes) were prepared to conduct compressive strength tests (Fig.4).

Figure 4: Uniaxial test with (a) a damaged concrete cube, (b) a concrete cube repaired with epoxy resin (Issa and Debs, 2007)

The results of the compressive tests (Table 1), indicate that the damaged concrete cubes had 32.71% to 40.93% less strength than the intact samples. The injection of epoxy allowed recovering almost 50% of the strength of the damaged samples. This shows that

the mechanical integrity of concrete structures may be jeopardized in the absence of remediation.

Table 1: Compressive strength of concrete cubes (Issa and Debs, 2007)

Crack Type	f'_c (MPa)	Reduction %	Status of cube
Intact concrete	33.0	-	-
Crack 1	19.1	40.93	2
Crack 2	22.2	32.71	3
Crack 1 + Epoxy	29.3	11.25	4
Crack 2 + Epoxy	30.3	8.23	5

I.A. Basunbul et al (1990) assessed epoxy remediation techniques by testing reinforced concrete beams, 150 x 150 mm in cross section and 1250 mm in length. Simply supported beams were subjected to a four-point loading. A 2.5 kN incremental load was applied on the top of the beam, at the center. Only major cracks (larger than 0.3mm) were repaired by epoxy adhesives, while fine cracks were not repaired. The beams were left for 7 days to ensure epoxy hardening after the injection.
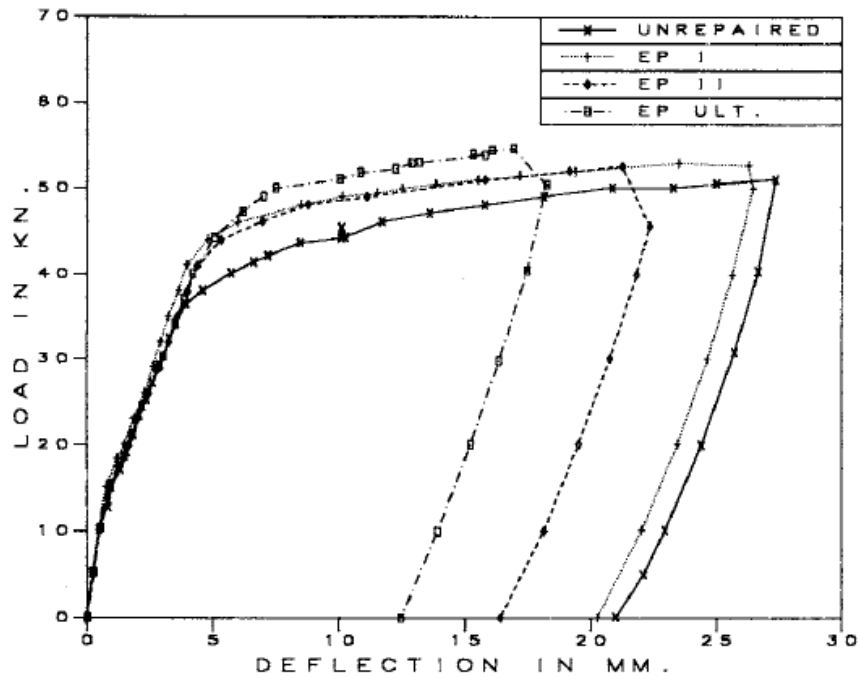
Figure 5: Load versus central deflection for beams repaired with epoxy injection (I.A. Basunbul et al, 1990)

Figure 5 shows the load versus deflection curves obtained by I.A. Basunbul et al. (1990) for the beams repaired with epoxy adhesives. Is was noted that repaired beams experience 50% less deflection than non-repaired beams, and that epoxy injection did not increase the ultimate load of the damaged beam. However, similar tests conducted on three specimens by Carolyn Dry et al (2016) showed that the load capacity of repaired concrete beams was in average equal to 133% of that of non-repaired concrete beams (Table 2). Deflection at the failure point was tremendously increased after epoxy injection, except for specimen A. These experiments confirm that the injection of epoxy resins could restore some of the structural integrity of damaged concrete beams.

Table 2: Load, deflection and relative stiffness of specimens (Carolyn Dry et al, 2016). Test 1: without epoxy. Test 2: with epoxy.

Adhesive Type	Specimen	Load (kN)			Deflection at failure (mm)		
		Test 1	Test 2	Change %	Test 1	Test 2	Change %
Epoxy resin	A	2.3	2.5	109%	3.9	3.8	-3
	B	1.9	2.7	142%	0.8	3.7	363
	C	2.4	3.5	146%	0.9	4.2	367

Due to the sensitivity of epoxy to temperature and fatigue loading, many studies have been performed to evaluate the structural performance of concrete structures repaired by epoxy injection under service loading, e.g., Al-Mandil et al (1990), EL-Hawary and Fattah (2000), Hong-Chol Shin et al (2011). Figure 6 shows the geometry of the specimen tested under cyclic loading by Hong-Chol Shin et al (2011). Two types of epoxy adhesives (hard and soft) were used.
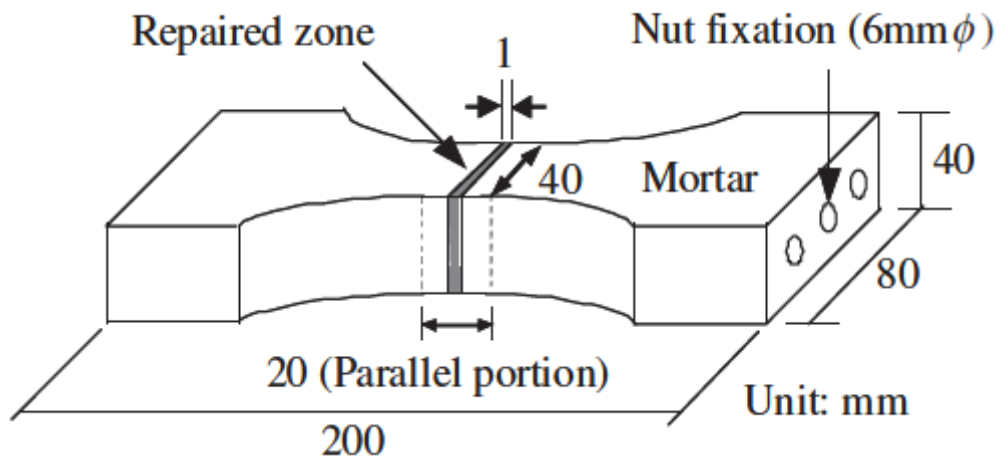
Figure 6: Dimensions of repaired concrete specimens by epoxy resins (Hong-Chol Shin et al, 2011)

The strain of the repaired sample was measured at four different temperature levels (5℃, 20℃, 30℃, and 40℃). A comparison between the results obtained with hard and soft epoxy (Figure 7) shows that hard resins do not experience significant deformation below 30C, whereas soft resins are highly sensitive to temperature changes, even below 30C.
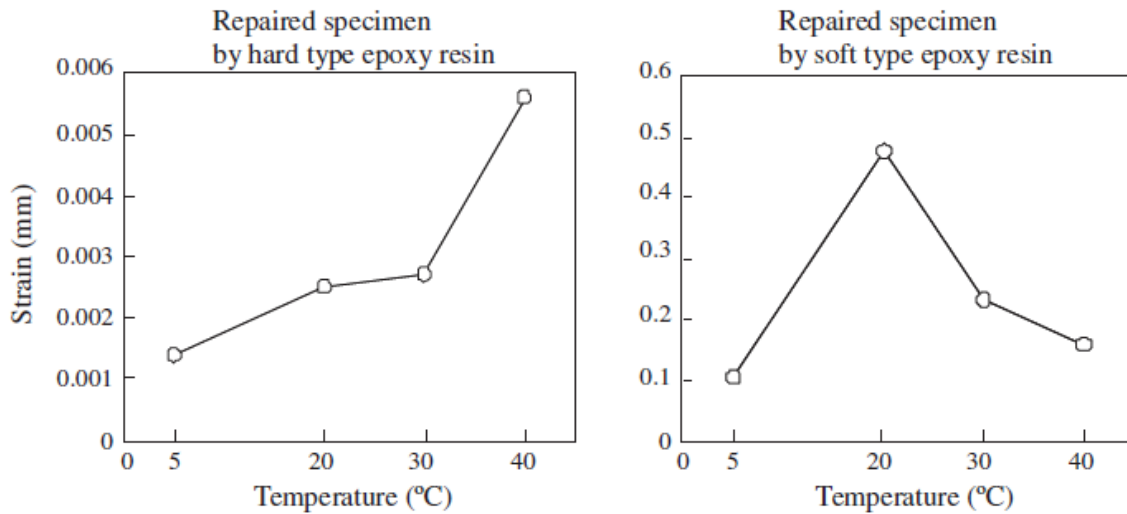
Figure 7: Results of fatigue tests performed on concrete repaired by epoxy (Hong-Chol Shin et al, 2011)

Repetitive displacement-controlled tests indicate that the resistance to fatigue significantly decreases owing to temperature effects, in both the hard and soft epoxy resins. Experimental results also confirm that fatigue in epoxy increases with the magnitude of displacement loadings. Finite Element analyses remain necessary to simulate long-term cyclic loading under temperature changes and assess the integrity and sustainability of pre-stressed concrete girder repaired by epoxy resins.
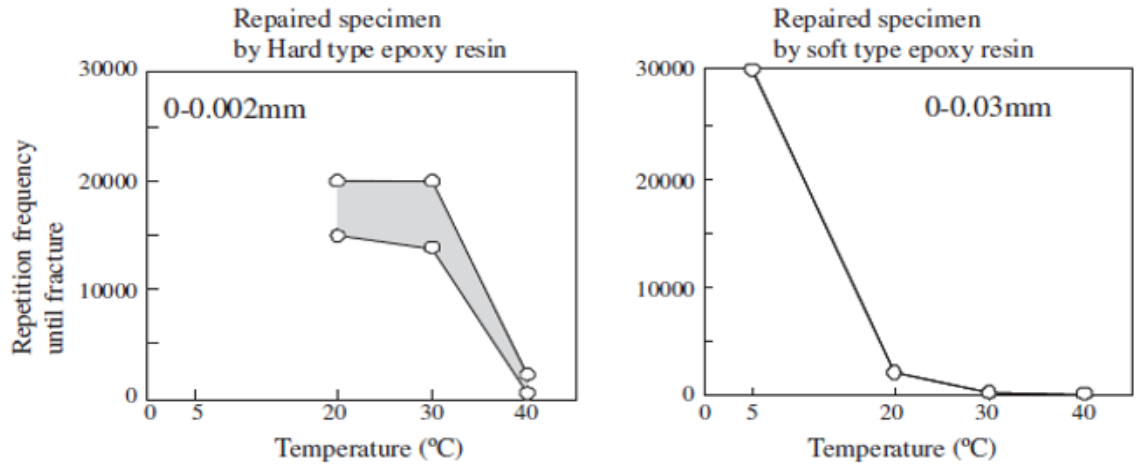
Figure 8: Number of loading cycles until failure in concrete samples: (a) repaired by hard epoxy resin, (b) repaired by soft epoxy resin (Hong-Chol Shin et al, 2011)

3. CONCRETE PROPERTIES

Because concrete is used in construction for its compressive resistance, concrete strength tests have been extensively used to evaluate concrete mechanical performance. Common laboratory experiments include uniaxial, biaxial, and triaxial tests. In the following, triaxial compression tests performed under various confinement pressures are used to calibrate a continuum damage mechanics model, the Differential Stress Induced Damaged (DSID). The DSID model allows predicting crack-induced mechanical anisotropy, stiffness and strength reduction and accumulation of inelastic strains (Xu and Arson. 2014). The data is taken from the work published in Imran (1994), Xie et al. (1995) and Candappa et al. (2000)

3.1 DIFFERENTIAL STRESS INDUCED DAMAGE (DSID) MODEL

In the following, the governing equations of the DSID model are summarized. The damage variable is a second order tensor (noted Ω), which is used to model the distribution of micro-crack planes present in a Representative Elementary Volume (REV), as follows (Fig 9):

$$\Omega = \sum_{I=1}^{3} d^I n^I \otimes n^I$$

In which n^I is the vector normal to the I-th principal crack plane, d^I is the volume fraction of cracks that are in the plane of normal n^I. The Gibbs free energy G_s is expressed as follows:

$$G_s(\sigma, \Omega) = \frac{1}{2}\sigma : S_0 : \sigma + a_1 Tr\Omega(Tr\sigma)^2 + a_2 Tr(\sigma \cdot \sigma \cdot \Omega) + a_3 Tr\sigma Tr(\Omega \cdot \sigma) + a_4 Tr\Omega Tr(\sigma \cdot \sigma)$$

Where σ is the stress tensor and a_i are material parameters (determined from numerical calibration in the next section). S_0 is the initial undamaged compliance fourth-order tensor. The total deformation tensor is split as follows (Fig9):

$$\varepsilon = \varepsilon^{el} + \varepsilon^{ed} + \varepsilon^{id} = \varepsilon^E + \varepsilon^{id}$$

In which ε^{el} is the purely elastic strain (which would be obtained in the absence of damage), ε^{ed} is the elastic damage-induced strain that results from the degradation of mechanical stiffness, and ε^{id} is the irreversible strain.
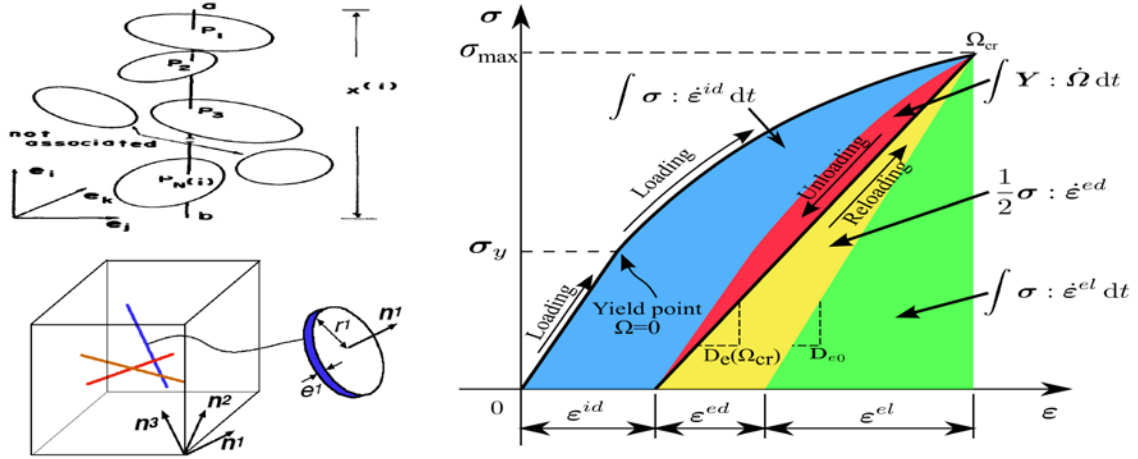
Figure 9: Representation of the damage variable (left) and schematic stress/strain curve (right) in the DSID model (Xu and Arson, 2014)

A hyper-elastic framework is adopted. Accordingly, the thermodynamic conjugation relationships are:

$$\varepsilon^E = \varepsilon - \varepsilon^{id}(\Omega) = \frac{\partial G_s}{\partial \sigma} = \frac{1+v_0}{E_0}\sigma - \frac{v_0}{E_0}(Tr\sigma)\delta + 2a_1 Tr\Omega(Tr\sigma)\delta\frac{1}{2}$$
$$+ a_2(\sigma \cdot \Omega + \Omega \cdot \sigma) + a_3[Tr(\Omega \cdot \sigma)\delta + Tr(\sigma)\Omega] + 2a_4(Tr\Omega)\sigma$$

$$Y = \frac{\partial G_s}{\partial \Omega} = a_1 (Tr\sigma)^2 \delta + a_2 \sigma \cdot \sigma + a_3 (Tr\sigma)\sigma + a_4 Tr(\sigma \cdot \sigma)\delta$$

Where E_0 and ν_0 are Young's modulus and Poisson ratio of initial undamaged material. δ is the identity tensor. The damage criterion is similar to a Drucker Prager yield function, in which stress is replaced by energy release rate, which is the work-conjugate of damage. The Drucker-Prager damage function allows predicting the evolution of damage with deviatoric stress and distinguishes tension and compression damage:

$$f_d = \sqrt{J^*} - \alpha I^* - k$$
$$J^* = \frac{1}{2}(P_1 : Y - \frac{1}{3}I^* P_1 : Y):(P_1 : Y - \frac{1}{3}I^* \delta)$$
$$I^* = (P_1 : Y):\delta$$

C_0 is the initial damage threshold, C_1 is an isotropic hardening variable, $H(\cdot)$ is the Heaviside function and $\sigma^{(p)}$ is the p-th principal stress. The irreversible strain is calculated from an associated flow rule as:

$$\dot{\varepsilon}^{id} = \dot{\lambda}_d \frac{\partial f_d}{\partial \sigma} = \dot{\lambda}_d \frac{\partial f_d}{\partial Y} : \frac{\partial Y}{\partial \sigma}$$

In order to satisfy the positivity of dissipation, the damage flow rule is chosen as non-associate:

$$\dot{\Omega} = \dot{\lambda}_d \frac{\partial g_d}{\partial Y}$$

In which $\dot{\lambda}_d$ is the Lagrangian Multiplier, and:

$$g_d = \sqrt{\frac{1}{2}(P_2 : Y) : (P_2 : Y)} - C_2$$

$$P_2(\sigma) = \sum_{p=1}^{3} H[\max_{q=1}^{3}(\sigma^{(p)}) - \sigma^{(p)}]n^{(p)} \otimes n^{(p)} \otimes n^{(p)} \otimes n^{(p)}$$

3.2 DSID MODEL CALIBRATION FOR CONCRETE

Results of triaxial compression tests performed by Candappa et al. (2001) are used as reference to calibrate the DSID model for concrete. An iterative algorithm was programmed in MATLAB to select the DSID parameters that minimize the least-square distance between experimental and numerical stress/strain curves. The main governing equations are as follows:

$$S = \sum_{i=1}^{n} r_i^2$$

$$r_i = y_i - f(x, B)$$

$$B_{n+1} = B_n - \gamma_n df(B_n)$$

S is the residual distance between experimental results y_i and numerical predictions $f(x, B)$. x is the vector of input data (e.g., strain for a displacement-controlled test, stress for a force-controlled test). B is the vector of unknown parameters, calculated to minimize S. The parameters found for concrete used in girders are listed in Table 3, and the stress/strain curves obtained by simulating the triaxial compression tests with the calibrated parameters are shown in Figure 10.

Table 3: Calibrated DSID parameters for concrete

Elasticity			Free energy			Damage function		
E_0 GPa	υ -	a_1 GPa^-	a_2 GPa^-	a_3 GPa^-	a_4 GPa^-	α -	C_0 MPa	C_1 MPa
28.96	0.21	11.26 $\times 10^-$	7.038 $\times 10^-$	-5.30 $\times 10^-$	35.86 $\times 10^-$	0.0267	0.001	0.0073

Figure 10: Concrete triaxial stress-strain curves. Experimental results from (Candappa et al, 2001). Numerical results obtained with the DSID model after calibration.

3.3 FINITE ELEMENT MODEL OF CONCRETE

The Differential Stress Induced Damage (DSID) model was implemented in ABAQUS Finite Element software, within a user material subroutine file. The DSID UMAT subroutine in ABAQUS was used to simulate uniaxial and triaxial compression

tests performed on concrete cubes of dimensions $200\text{mm} \times 200\text{mm} \times 200\text{mm}$. We compared two Finite Element models:

- In model 1 (Fig 11), the concrete cube is placed between the two steel plates, like in the experiment performed by Issa and Debs (2007). A friction coefficient of 0.6 is chosen to represent the contact between the steel plates and the concrete (B. G. Rabbat et al. 1985). A vertical stress is applied on the top plate, and the bottom plate is fixed in all directions.

- In model 2 (Fig 12), the displacements of the center of the bottom face is fixed in x, y and z directions. The vertical displacement is fixed to zero at all other nodes of the bottom face.

In both models, confinements stresses of 1.05MPa, 4.2MPa, and 8.4MPa are applied on the sides. Below are the notations adopted in Figures 11 and 12.

U1: displacement in x direction	**UR1: rotation about x axis**
U2: displacement in y direction	**UR2: rotation about y axis**
U3: displacement in z direction	**UR3: rotation about z axis**
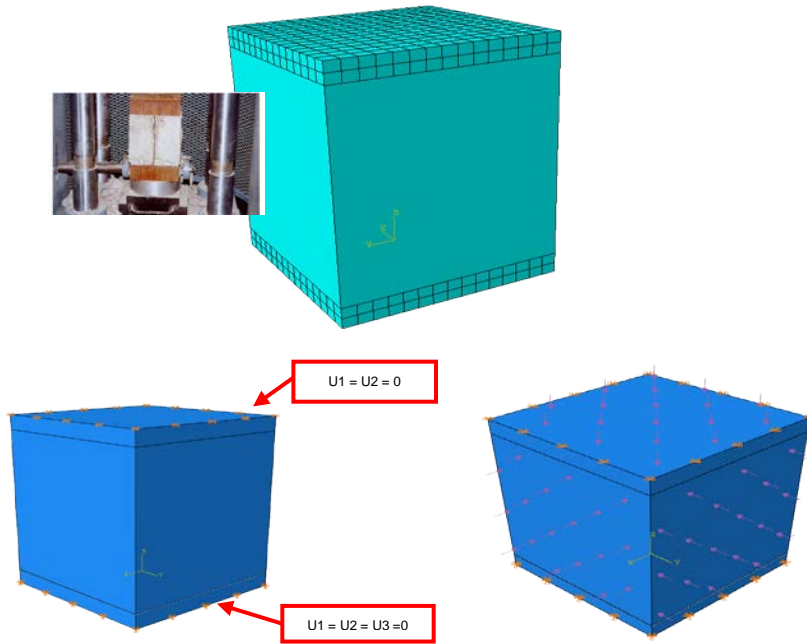
Figure 11: Boundary conditions adopted in the compression tests (Model 1)
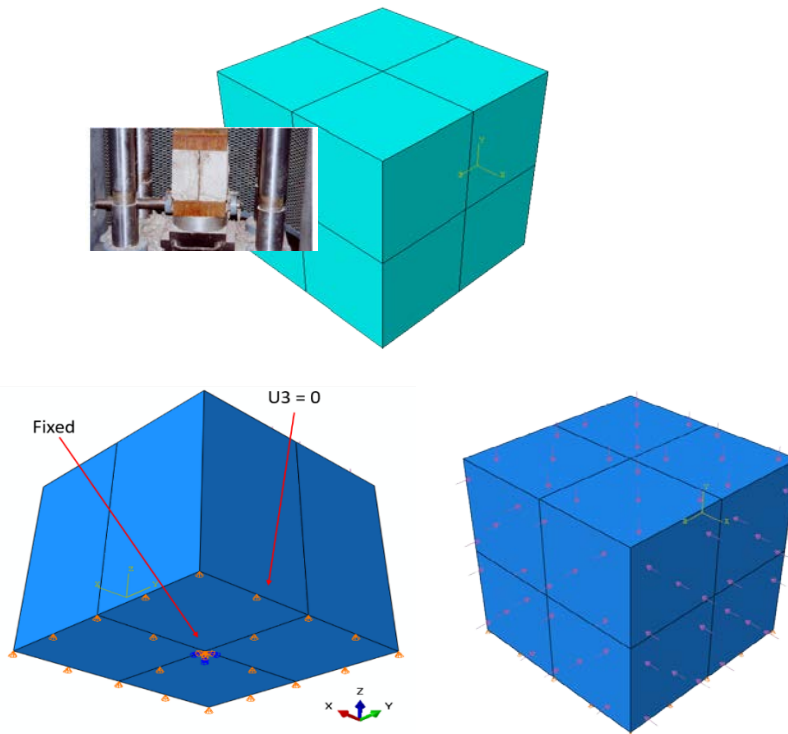
Figure 12: Boundary conditions adopted in the compression tests (Model 2)

Stress-strain curves obtained with MATLAB and with the two FEM models are presented in Figure 13, and the corresponding evolution of damage with the deviatoric stress is shown in Figure 14. In Model 1, friction between concrete and the steel plates induces stress concentrations. In model 2, the stress applied at the top boundary represents what is actually applied during the experiment. That is why less damage is observed in the simulations done with Model 1. As expected, the results provided by Model 2 are closer to those obtained with the MATLAB code, which calculates concrete stresses and strains at the material point and does not account for boundary conditions.
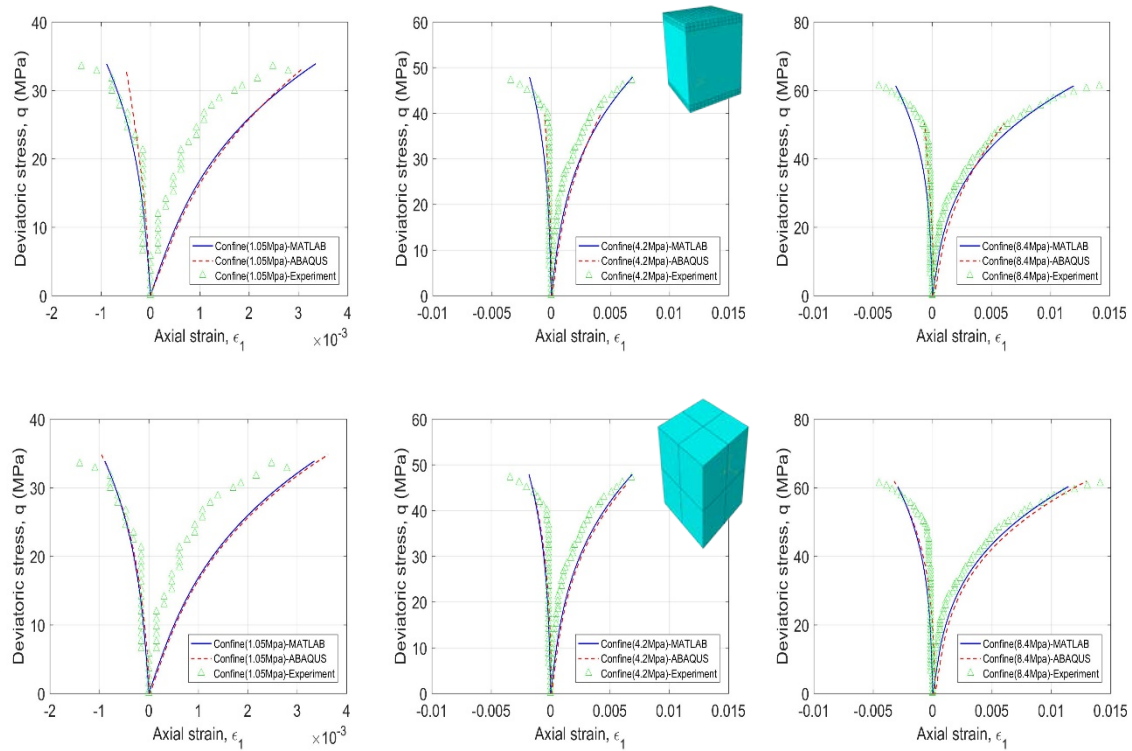
Figure 13: Stress/strain curves obtained by simulating compression tests performed on a concrete cube under a confining stress of: (a) 1.05Mpa (b) 4.2Mpa (c) 8.4Mpa (Top: Model 1; Bottom: Model 2)
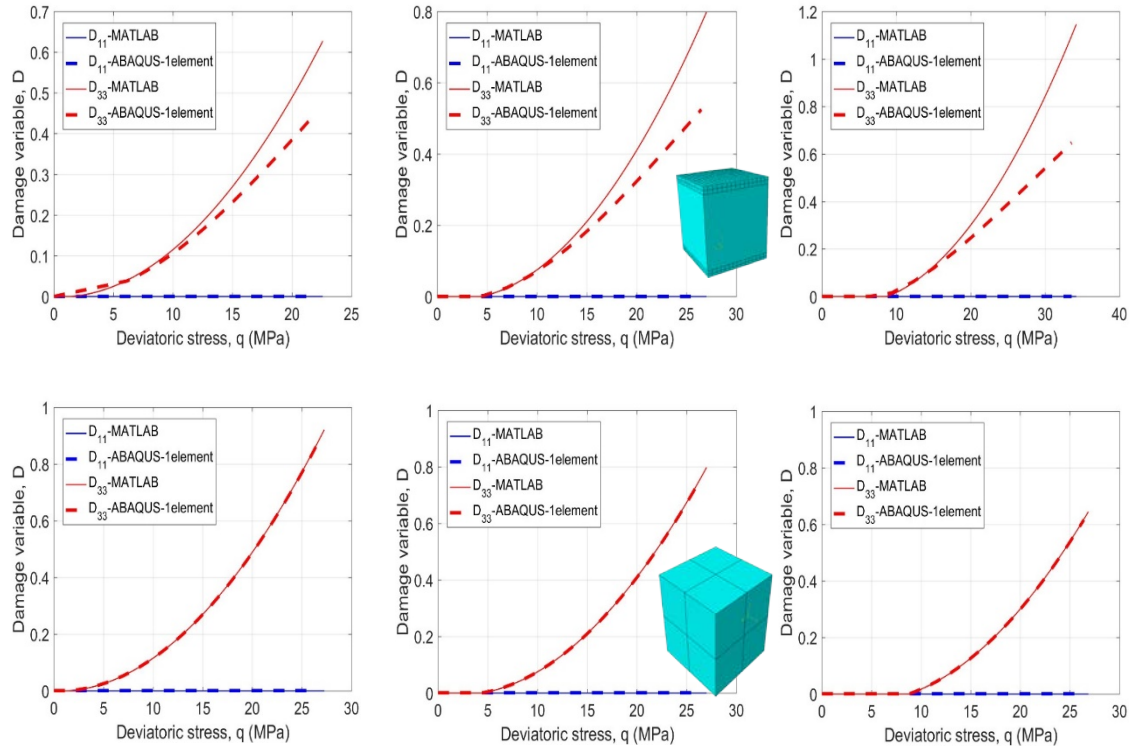
Figure 14: Evolution of damage during the compression tests performed on concrete cube with a confinement stress of: (a) 1.05Mpa (b) 4.2Mpa (c) 8.4Mpa (Top: Model 1, Bottom: Model 2)

In order to analyze the sensitivity of the stiffness model to damage changes, uniaxial compression tests were simulated with Model 2 boundary conditions, with different values of initial damage in the vertical direction (Ω=0.0, 0.1, 0.2). This initial damage represents longitudinal cracks (in planes that have a vertical normal vector). A vertical stress of 33 MPa was applied on the top face. As expected, vertical displacements are higher and van Mises stress is lower for higher values of the initial damage (Fig. 15 and 16). These simulations show the importance of initial damage on concrete behavior, and potentially, the importance of longitudinal cracks induced by pre-stress relaxation on the mechanical behavior of steel-reinforced concrete subject to service loads.
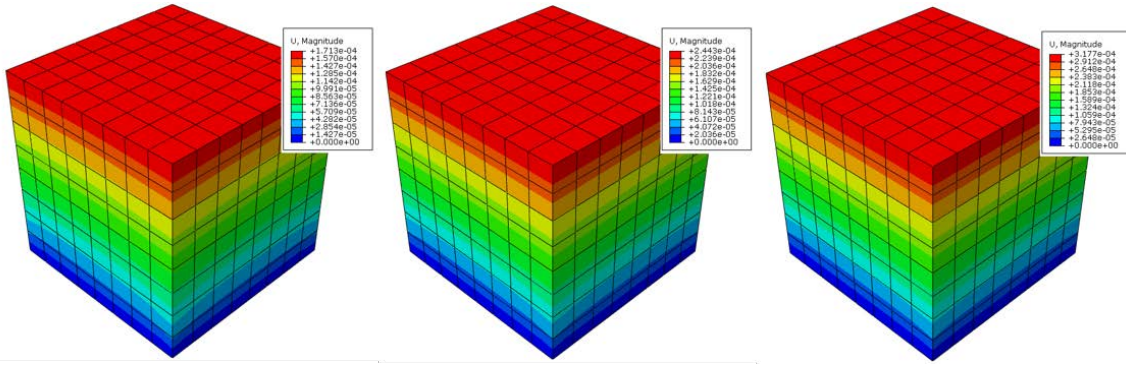
Figure 15: Vertical displacement in the concrete cube with different values of initial damage representing longitudinal cracks: (a) Ϫ=0 (b) Ϫ=0.1 (c) Ϫ=0.2
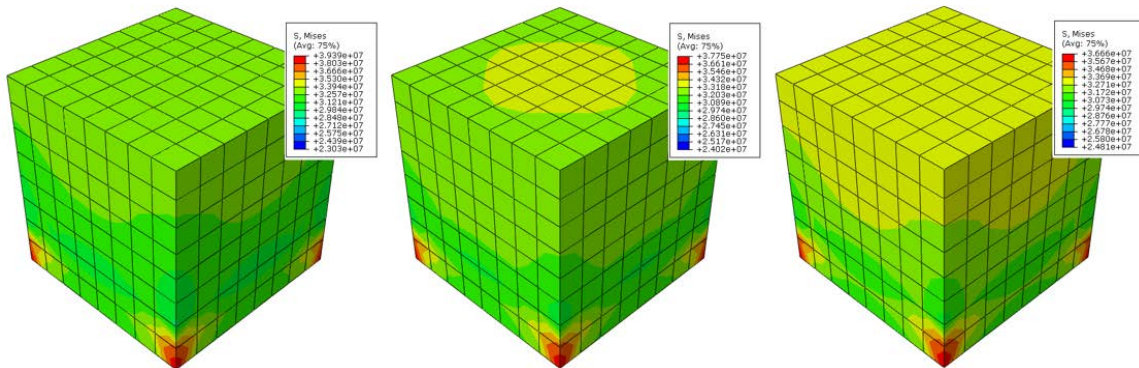
Figure 16: Van Mises stress in the concrete cube with different values of initial damage representing longitudinal cracks: (a) Ϫ=0 (b) Ϫ=0.1 (c) Ϫ=0.2

4. NUMERICAL ANALYSIS OF STRESS AND DAMAGE IN A BRIDGE DECK SUPPORTED BY PSC GIRDERS

4.1 PRE-STRESSED CONCRETE GIRDER GEOMETRY AND BOUNDARY CONDITIONS

We design a Finite Element model for a portion of bridge deck supported by pre-stressed concrete girders. The geometry of the structure, the design of the pre-stressed steel reinforcements and the materials' properties are taken from an example presented by the U.S Department of Transportation Federal Highway Administration (Fig 17-18, Table 5). The location of the reinforcing steel and pre-stressing strands are chosen according to the AASHTO Standard Specifications and AASHTO-LRFD Specifications. This typical example of bridge deck is made of two 110ft-long spans, placed on simply supported pre-stressed concrete girders that are aligned with the axis of the railroad. AASHTO TYPE VI Girders are used; they are 110ft long (i.e. girders have the same length as the span they support); the spacing is 9'- 8". Concrete Type F-Parapets 1' – 8 ¼" wide are chosen as railing. For the deck design, four 12 ft. wide lanes are considered.
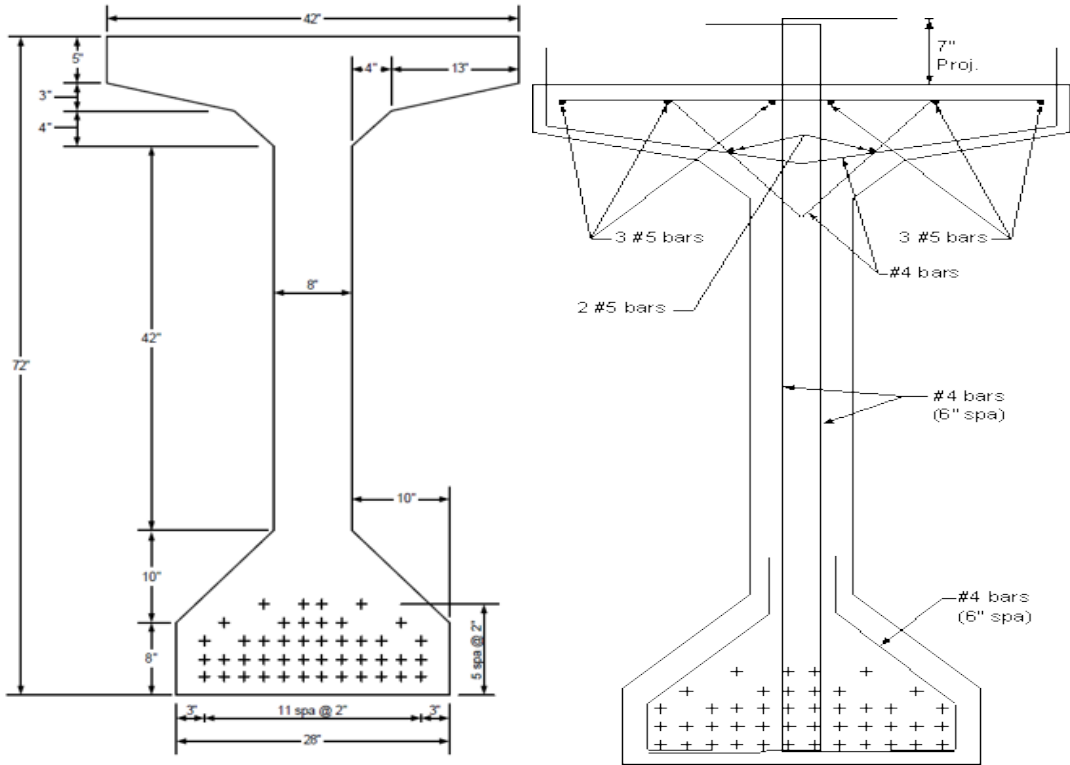
Figure 17. AASHTO TYPE VI Girders design (U.S Department of Transportation Federal Highway Administration)

Table 4: Properties of the materials used in the construction of the Example Bridge (U.S Department of Transportation Federal Highway Administration)

Concrete material properties	Concrete strength	Elastic modulus
Pre-stressed girders	6 ksi	4200 ksi
Deck slab	4 ksi	3934 ksi
Steel material properties	Yield strength	Elastic modulus
Reinforcing steel	60 ksi	28500 ksi
Pre-stressing strands	270 ksi	28500 ksi
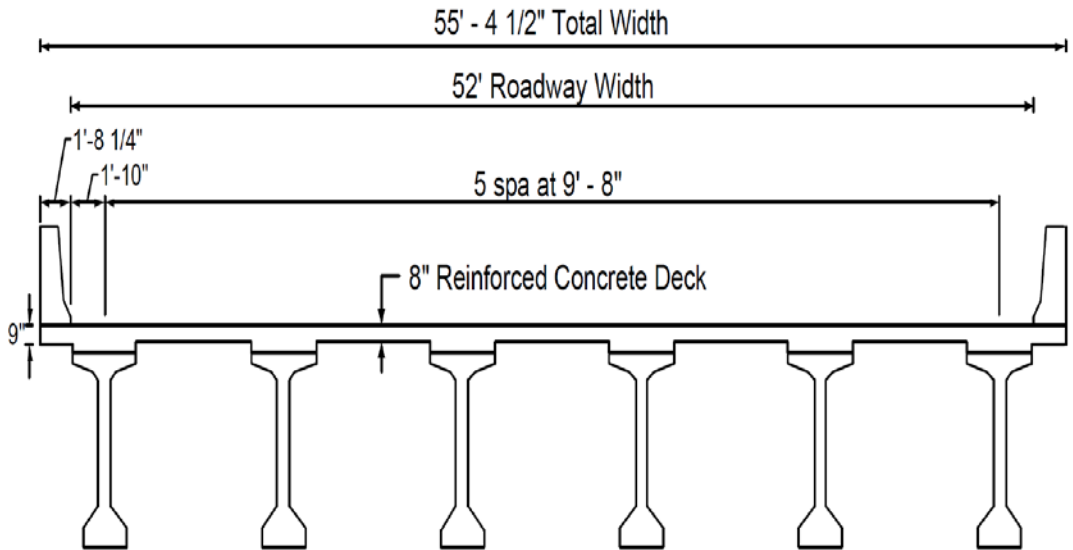
Bridge cross-section
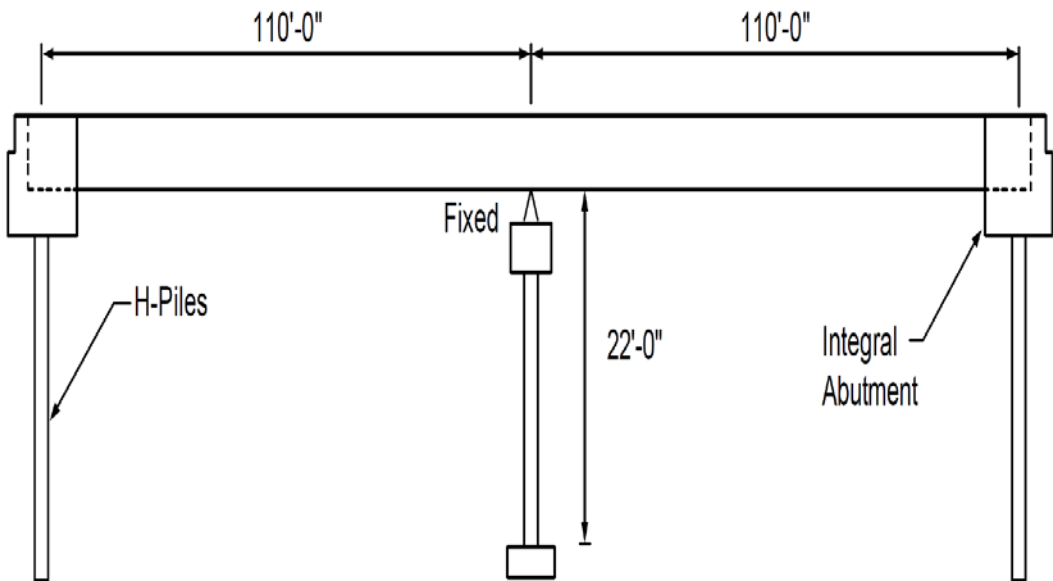
Elevation view of the example bridge

Figure 18. Example bridge geometry (U.S Department of Transportation Federal Highway Administration)

The mesh adopted in the Finite Element model is shown in Fig 19. Due to symmetries, only a half of the deck is modeled. The reinforcing steel was modeled with

25

truss elements. Concrete and rubber were modeled with volume elements (linear brick elements). The material properties of the reinforcing steel and of pre-stressed strands are given in Table 5. The shear modulus and Poison's ratio of the bearing pads were chosen so as to represent typical rubber behavior.
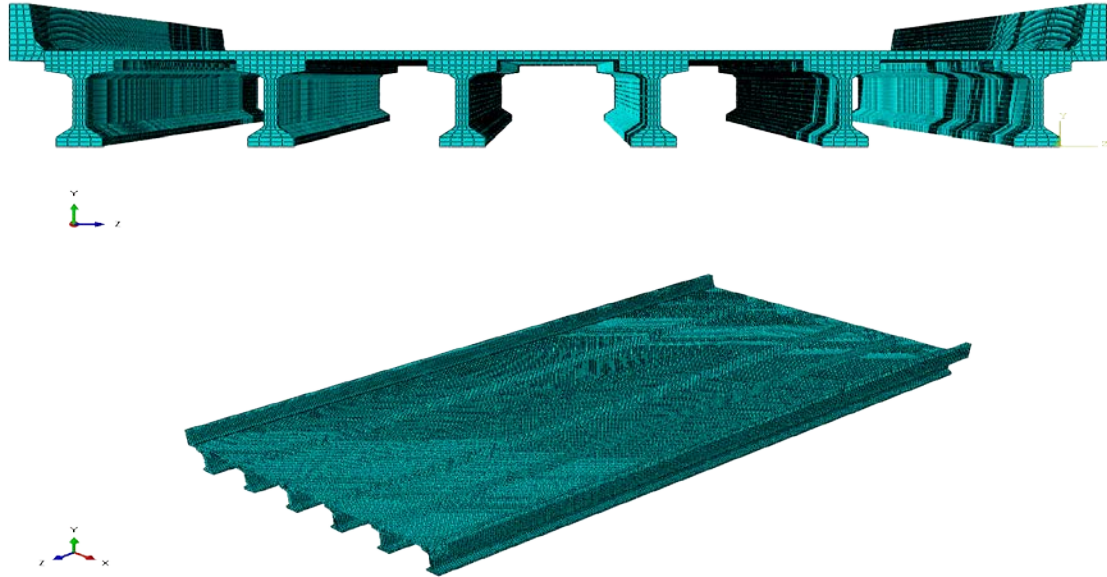
Figure 19. Mesh adopted in the Finite Element bridge model

Table 5: Loading conditions adopted in the bridge Finite Element model

Initial step	Step-1	Step-2
202.5 ksi	386.088 in/s^2	1.75 lbf/in^2

Figure 20 shows the FE model boundary conditions. The bearing pads are assigned zero displacements in x, y and z directions to simulate the presence of pillars. Note that zero displacements are assumed at the bottom of the rubber pads only, which implies that the

top of the pillar has zero displacement but the rubber pad can deform. Therefore the displacements at the top of the bearing pads are accounted for in the simulations presented in the following. Loading is applied in three steps: (1) pre-stress force of 202.5 ksi in the pre-stressing strands; (2) gravity forces accounting for the weight of the reinforcing steel, pre-stressing strands and concrete (yellow color arrows in Fig 20); (3) trucks load in the 4 lanes (plum arrows in Fig 20). In step 3, we assume that trucks fully occupy the 4 lanes, therefore, a $1.75 \text{lbf}/in^2$ stress is assigned on the top of the deck.
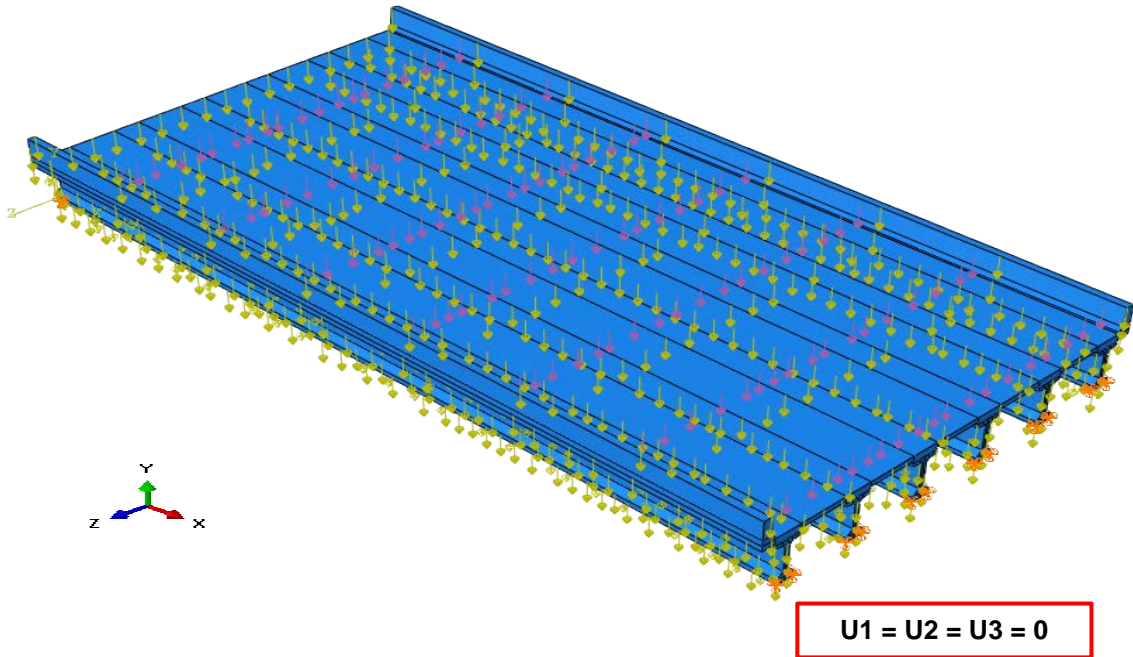
Figure 20. Boundary conditions adopted in the Finite Element model of bridge deck

U1: displacement of x direction	UR1: rotation of x axis
U2: displacement of y direction	UR2: rotation of y axis
U3: displacement of z direction	UR3: rotation of z axis

4.2 SIMULATION OF STATIC SERVICE LOAD WITH UNDAMAGED PSC GIRDERS

We first assume that the concrete is elastic. Fig 21 shows the results obtained with the elastic model. The maximum displacement, obtained at the center, corresponds to a 0.6212 inch deflection. The simulation results indicate that the anticipated deflection is negligible under static service load. The highest stress levels are found in the girder that is at the center of the deck.
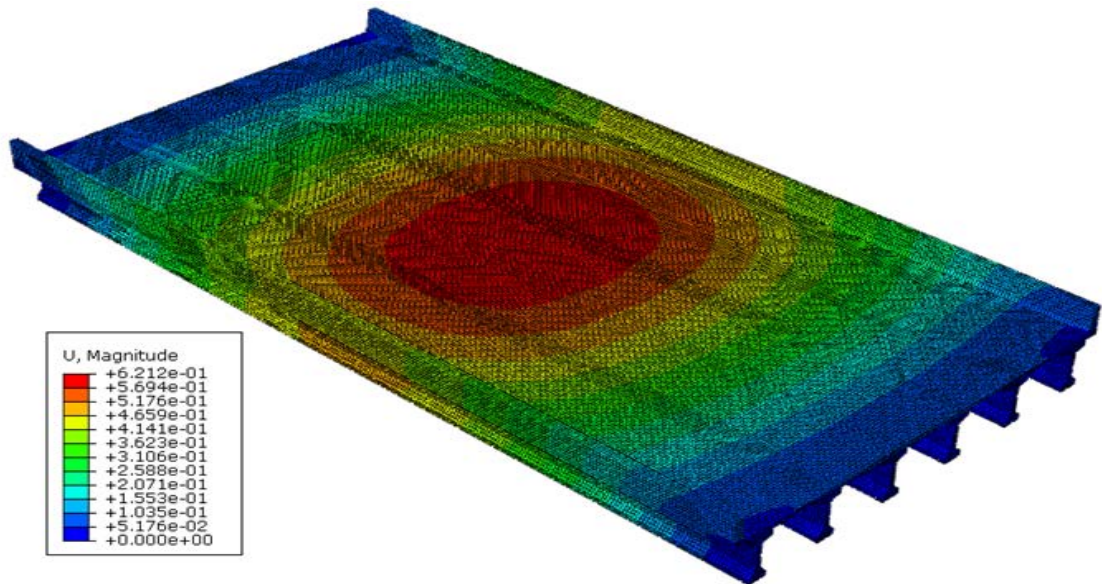
Figure 21: Displacement field in the pre-stressed concrete girder bridge (Elastic model)

4.3 DAMAGED PSC GIRDER SIMULATION

We now study the influence of crack propagation in the girders. The simulations are intended to predict the possible occurrence of damage during service loading. We choose to model damage propagation only in the girder at the extreme left of the model. All the concrete elements in that girder are assigned the DSID model (instead of an elastic model in the previous simulations). The other girders are made of elastic concrete. We use the DSID parameters obtained by calibration in Section 3.2. Results are shown in Fig. 22: horizontal damage (i.e., vertical cracks) in the pre-stressed concrete girder bridge concentrates around the bearing pads, which is consistent with in situ observations. The numerical model can thus capture the initiation and direction of cracks due to service loading. Convergence issues prevented us from calculating the final value of the damage variable. It is proposed to explore other damage modeling strategies in the subsequent phases of the project, e.g. a Cohesive Zone Model (CZM, see next sections).
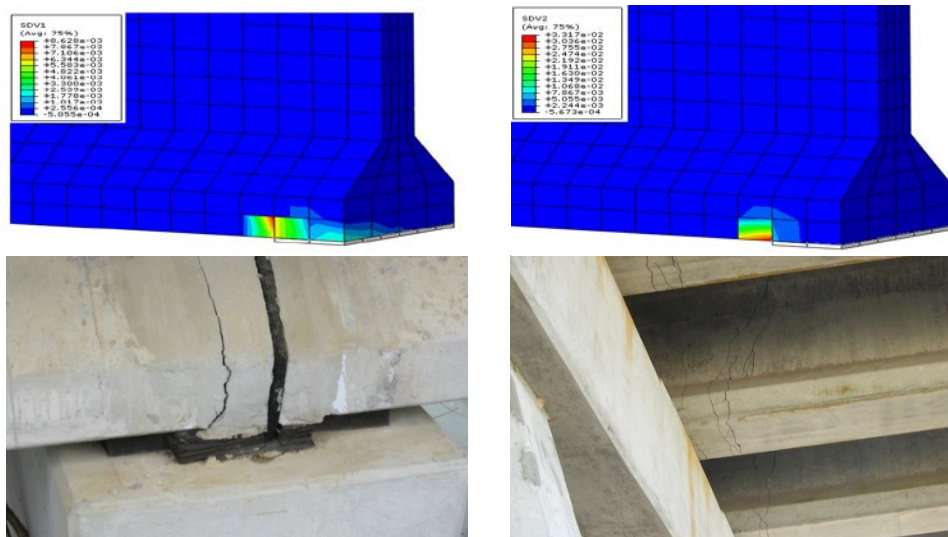
Figure 22: Distribution of damage due to the dead loads of trucks in the simulations (top) and in the field (bottom, after GDOT)

Now we simulate the influence of initial damage on the displacements and stresses close to the bearing pad in the damaged PSC girder. We study different crack orientations (i.e. different damage components) and different crack locations (i.e. different damaged elements). We assign an initial damage to the same number of Finite Elements (i.e. to the same volume of concrete) in all the simulations. Results are presented in Fig 23 -26. First, we account for initial damage due to service loading: we represent vertical cracks close to the bearing pads by assuming that the horizontal damage is non-zero in Finite Elements close to the pads (we compare $\Omega_{xx}=0, 0.1, 0.2$). Displacements and stresses are extracted from the nodes of the pre-damaged elements, and averaged over each element (Fig 23). As expected, displacements increase and stresses decrease as the initial damage is increased. Next, we study the influence of initial longitudinal (horizontal) cracks induced by pre-stress relaxation. Because the pre-stressed steel reinforcements are located on the bottom of the girder, the initial damage is assigned in this area. Results are shown in Fig 24. As expected, lower displacements are noted in the absence of initial damage. We also present two cases that represent crack patterns described in the PCI – Bridge Member Repair Guidelines: diagonal cracks in the web (Fig.25) and bottom cracks in the flange (Fig.26). Conclusions are similar to those drawn in the previous cases: the higher the initial damage, the higher the displacements, and the lower the stresses. We note that under the same amount of stress, vertical cracks at the bearing pads induce the higher displacement variations.
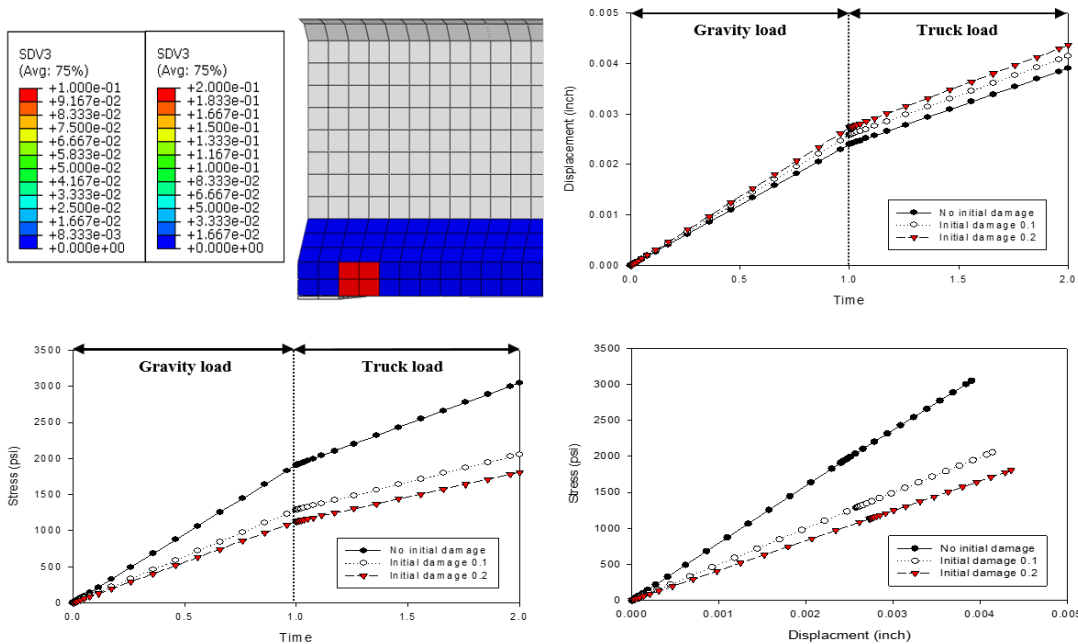
Figure 23: PSC girder around bearing pads with initial vertical cracks, i.e. horizontal damage (Ω=0, 0.1, 0.2)
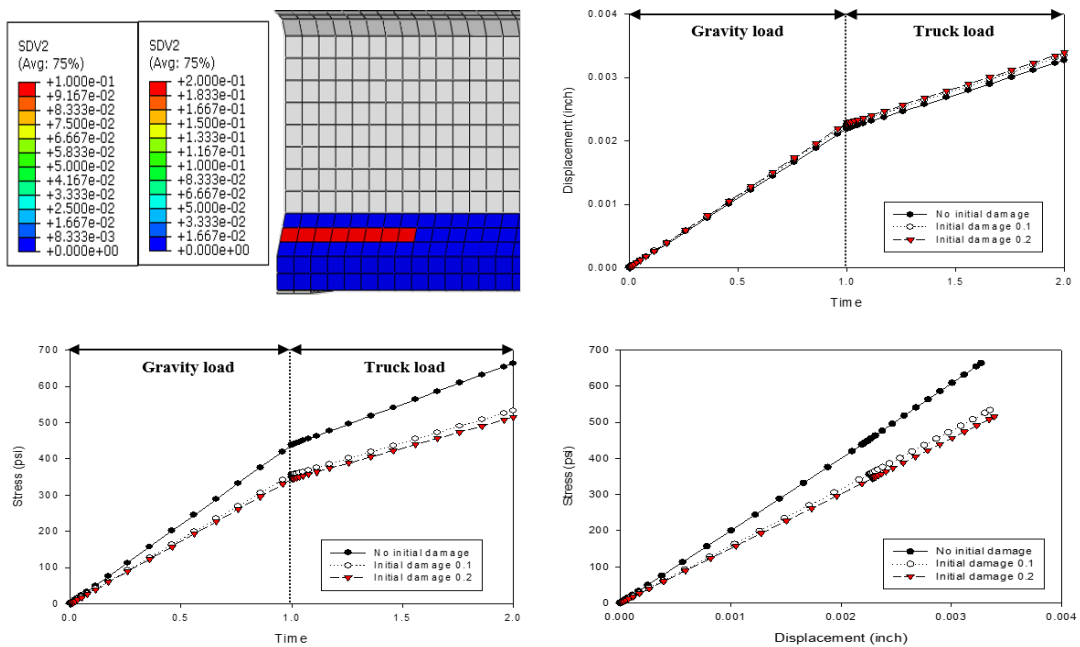
Figure 24: PSC girder around bearing pads with initial flange horizontal cracks, i.e. vertical damage (Ω=0, 0.1, 0.2)
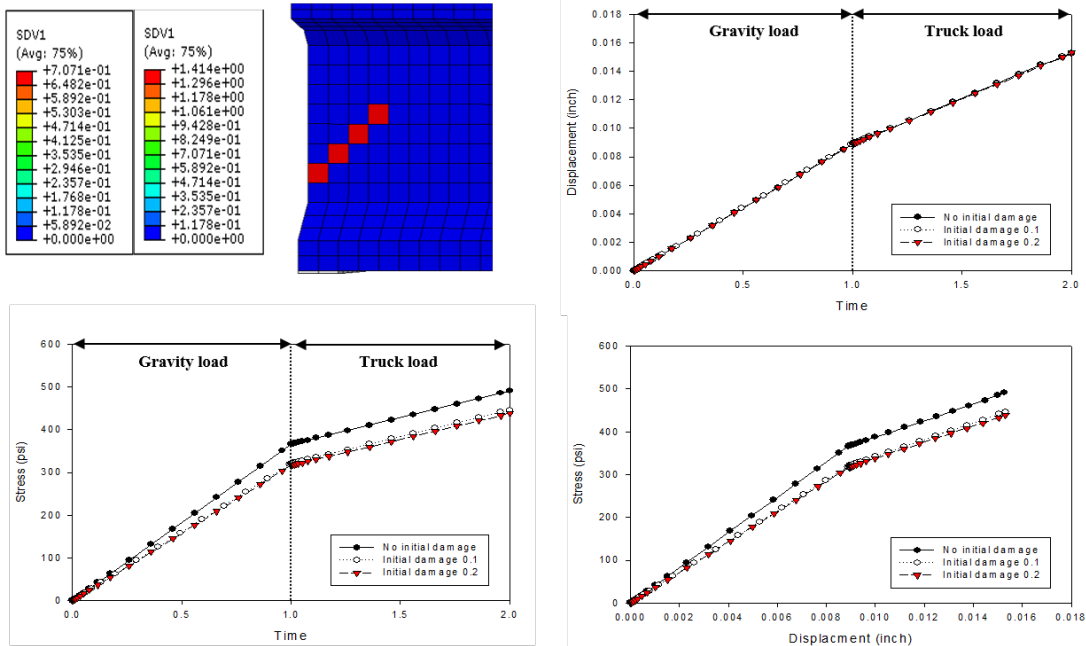
Figure 25: PSC girder around bearing pads with initial diagonal cracks (Ω=0, 0.1, 0.2)
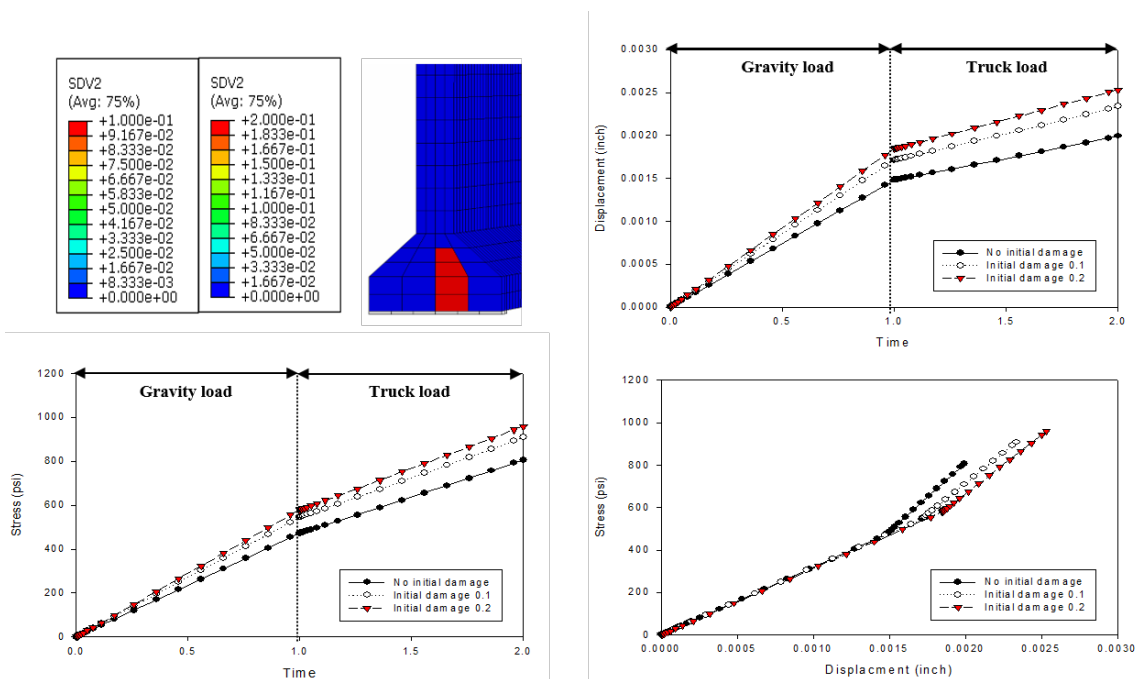
Figure 26: PSC girder around bearing pads with initial flange bottom cracks, i.e. vertical damage (Ω=0, 0.1, 0.2)

5 NUMERICAL STUDY OF THE EFFECT OF END ZONE CRACKING ON PSC GIRDERS STRESSES AND DISPLACEMENTS

In this section, we present Finite Element models of PSC girders used in Tennessee, Washington State, Virginia and Florida. We simulate load tests performed by Tadros et al. (2010) to assess the effect of cracks in the end zone of the girders, which are known to affect the flexural and shear capacities of pre-stressed girders. We compare the stress distributions and the deflection of the four types of girders with: no cracks; initial longitudinal cracks; initial vertical cracks; initial diagonal cracks; initial cracks in the bottom flange. The location and orientation of the initial cracks were chosen to comply with damaged cases listed in the PCI Bridge Member Repair Guidelines (PCI, 2012, PCINER-01-BMRG). Cracks were modeled with a non-zero damage value, like in the previous section.

5.1 DESCRIPTION OF THE TEST SPECIMENS AND BOUNDARY CONDITIONS

The four PSC girders used in the tests were 42-ft-long specimens that had the same number of strands than the girders used in actual bridges; they were designed according to the AASHTO LRFD Specification.

5.1.1 TENNESSEE GIRDER

Tennessee Specimens were 42-ft-long Type iii AASHTO I-girders and were fabricated by Construction Products, Inc. Each girder had thirty 0.5-in. diameter, 270si, low relaxation pre-stressing strands, stressed to 33.8 kips per strand. Figure 27 shows the details of the Tennessee specimens.
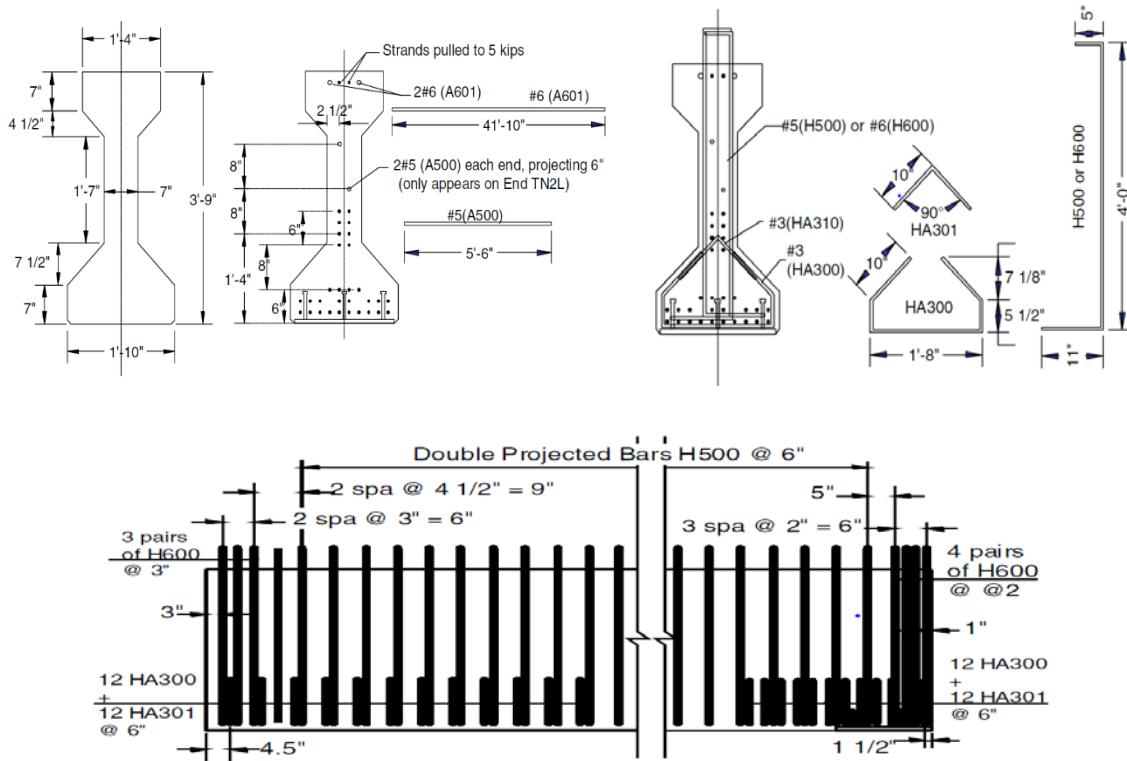
Figure 27: Details of the Tennessee Specimen. (Tadros et al., 2010).

5.1.2 WASHINGTON STATE GIRDER

Concrete Technology corporation of Tacoma, Washington, fabricated 42-ft-long, 58-in. deep girders. Thirty-eight straight 0.6-in. diameter, 270ksi, low relaxation pre-stressing strands were placed in the bottom portion of the girder. At the top of the girder, 20 additional pre-stressing steels 0.6-in diameter were included (Figure 28).
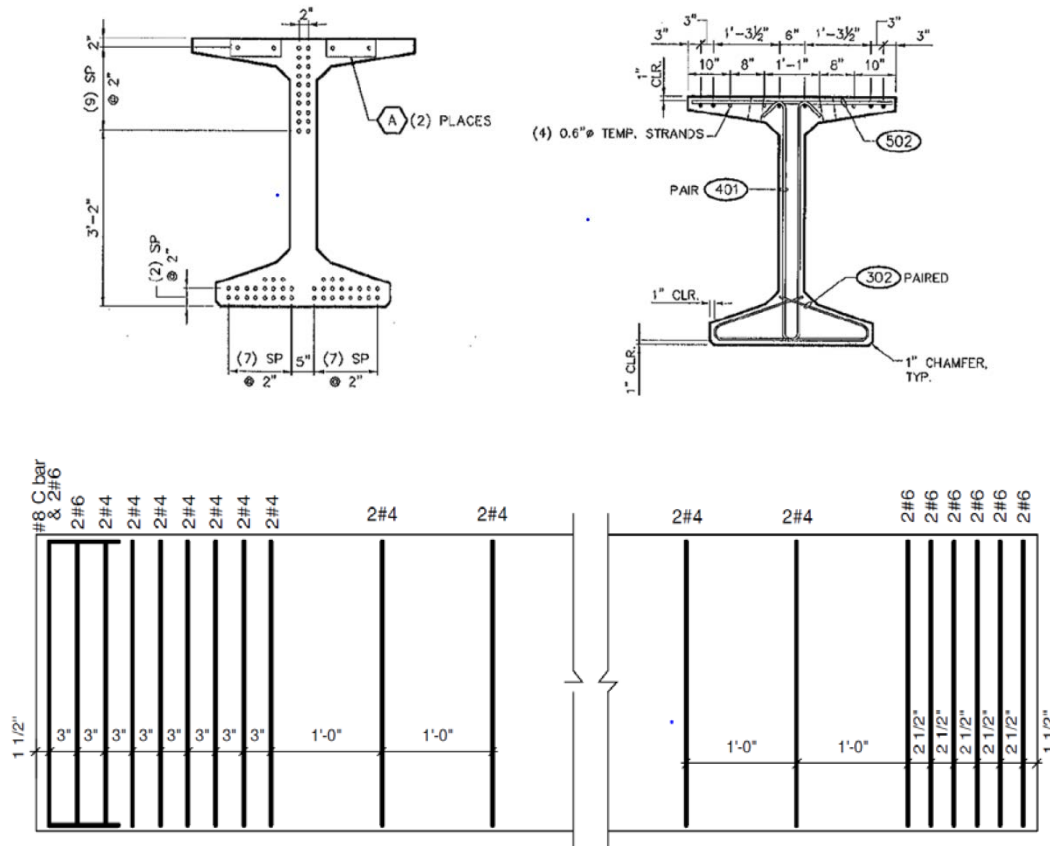
Figure 28: Details of the Washington State Specimen. (Tadros et al., 2010).

5.1.3 VIRGINIA GIRDER

Virginia Specimens were produced by Bayshore Concrete Products of Cape Charles, Virginia. Girders were 42-ft-long, 45-in. high Bulb-T girders with thirty-eight 0.6-in diameter, 270 ksi, low relaxation pre-stressing strands in the bottom flange and fourteen 0.6-in diameter 270ksi, low relaxation prestresssing strands in the top flange. Details are shown in Fig. 29.
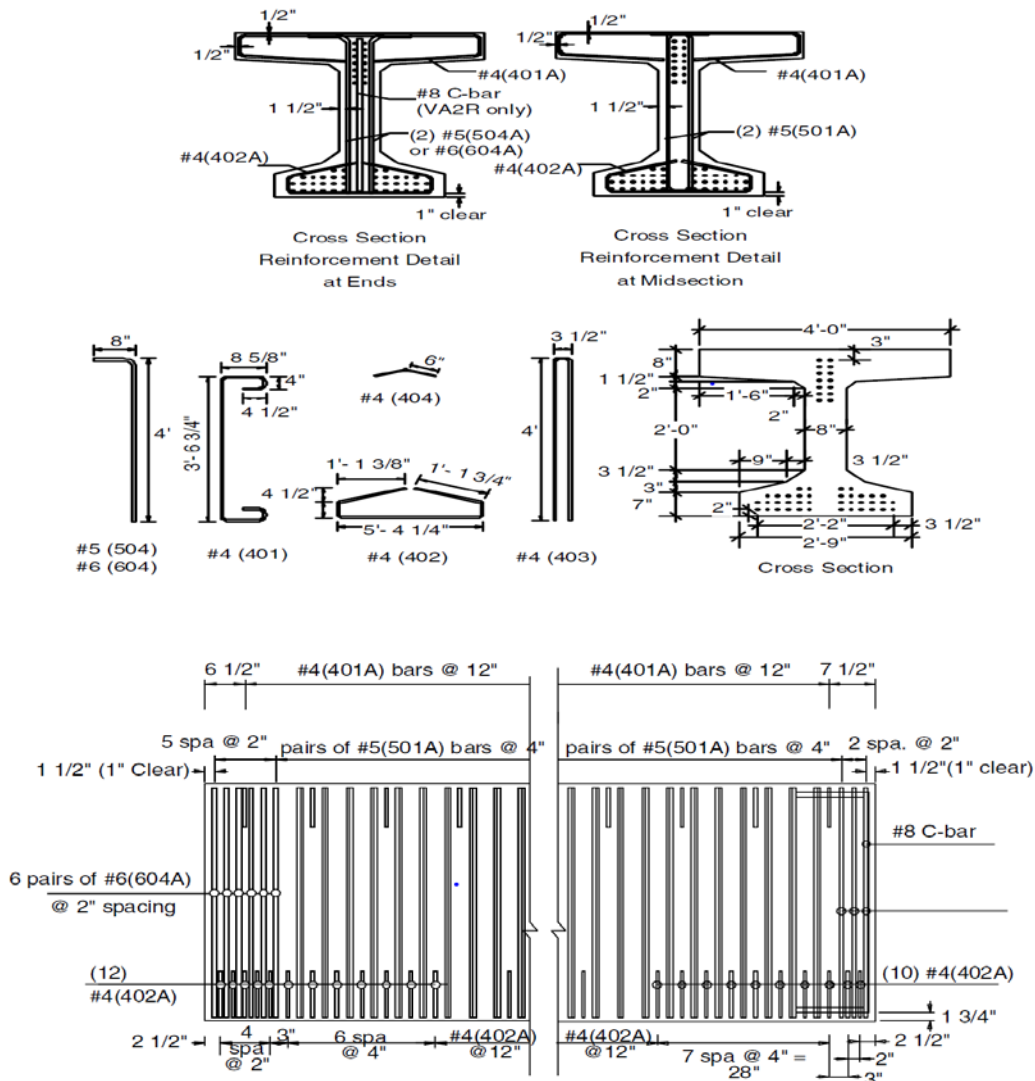
Figure 29: Details of the Virginia Specimen. (Tadros et al., 2010).

5.1.4 FLORIDA GIRDER

Standard Concrete Products of Tampa, Florida, fabricated 42-ft-long, 60-in deep inverted T girders. For the pre-stressing steel, thirty-six 0.6-in diameter, 270 ksi, low relaxation pre-stressing strands were used in the bottom flange, and six #6 bars were put along the top of the web. Details are shown in Fig.30.
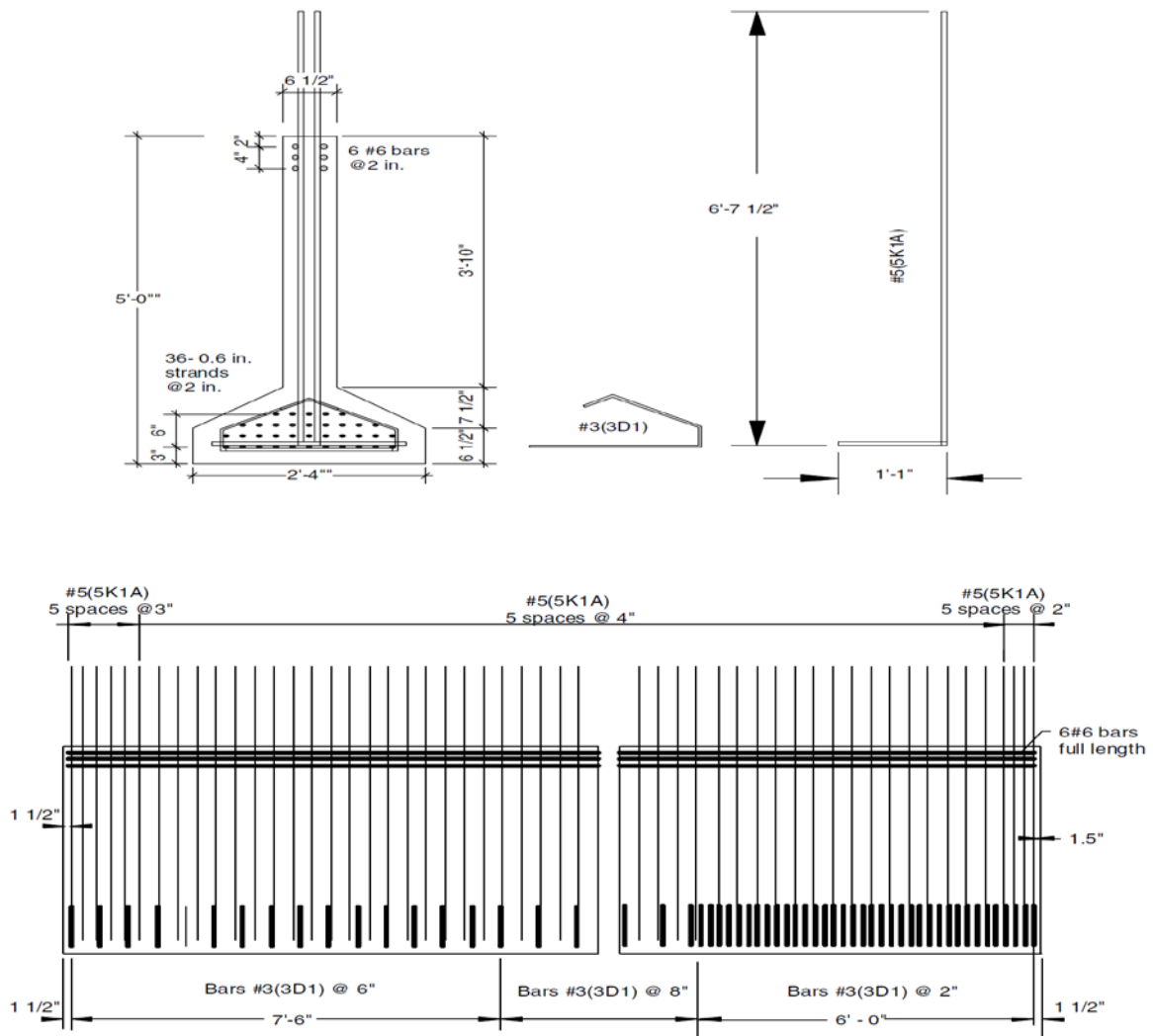
Figure 30: Details of the Florida Specimen. (Tadros et al., 2010).

5.1.5 BOUNDARY CONDITIONS

The boundary conditions adopted during the tests are shown in Fig.31. Specimens were supported at 6 in. from each end, leaving an unsupported length of 41 ft. A point load was applied at 12 ft. from the end being tested. A clamping force was applied by using a hydraulic jack in order to account for the dead loads that tend to close the end zone cracks.
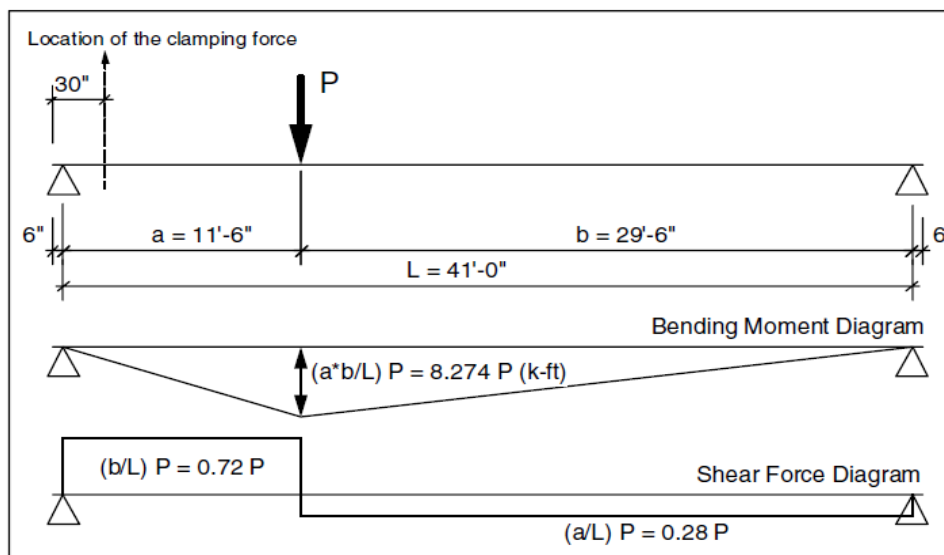
Figure 31: Loading and supports used in the full-scale girder load test (Tadros et al., 2010).

5.2 INITIAL DAMAGED PSC GIRDER FE SIMULATION RESULTS

We simulated the load test presented in Fig.35 for the four types of girders, with and without initial damage. The location and orientation of the initial cracks were chosen to comply with damaged cases listed in the PCI Bridge Member Repair Guidelines (PCI, 2012, PCINER-01-BMRG): initial longitudinal cracks; initial vertical cracks; initial diagonal cracks; initial cracks in the bottom flange (Fig.32). Simulations with initial damage were done with the same mesh as in the simulations without damage. We assigned a 0.5 damage value to 50 elements in each damaged girder model.
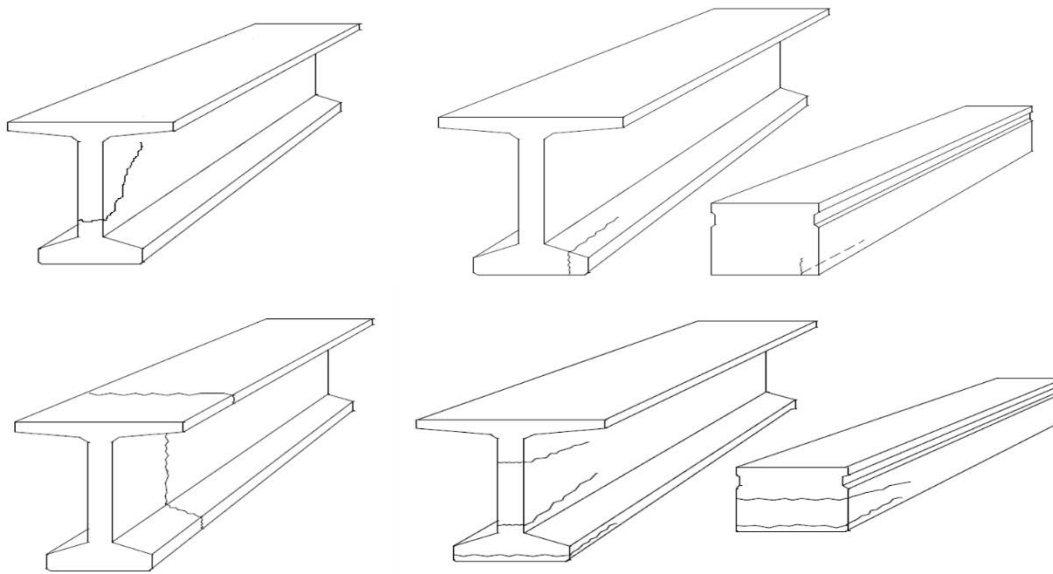
Figure 32: Typical end zone crack patterns (Bridge Member Repair Guidelines-PCI): (1) Diagonal crack (2) Flange Bot crack (3) Vertical crack (4) Longitudinal crack.

The simulation results are summarized in Figure 33 – 36. The main conclusions that can be drawn are the following:

- Vertical and shear stresses were not affected by the presence of initial damage (hence we plotted only the results obtained for undamaged girders).

- Peak values of shear and vertical stress were obtained at the points of application of the clamping and loading forces in all simulations.

- The effect of initial cracks on deflection was minimal; increased displacements were only noted in the area close to the point of application of the clamping force.

- The shape of the deflection curve was the same in all cases simulated. The maximum vertical displacement was between 0.3 inches (Tennessee girder) and 1 inch (Florida girder), and was obtained at a distance ranging between 240 and 280 inches from the cracked end of the girder.

- Virginia and Florida girders were the least affected by the presence of cracks.

- The most noticeable effects on deflection were obtained for vertical and diagonal cracks.

In order to improve the prediction of stress concentrations and loss of bearing capacity induced by end cracks, it is recommended to verify and expand the results by using a discrete fracture model. Accordingly, the principles of the Cohesive Zone Models (CZM) are presented in the next section.
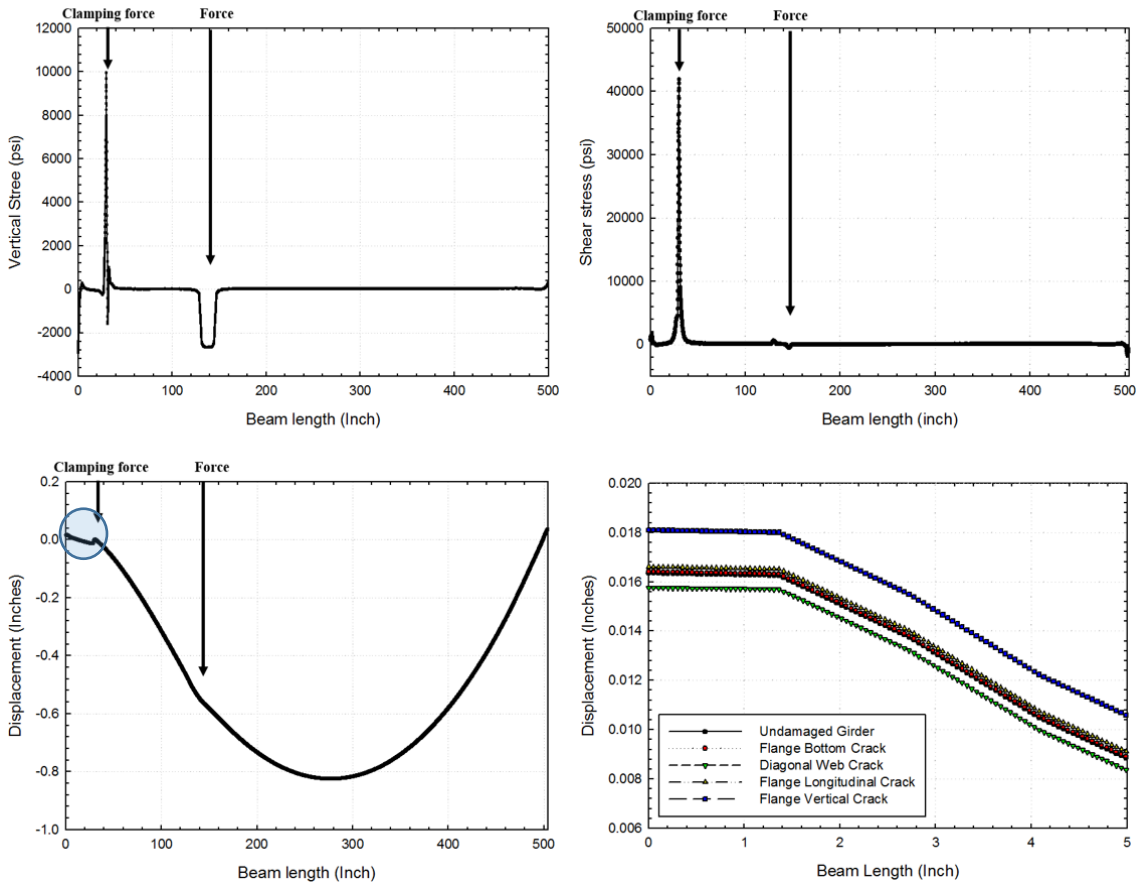
Figure 33: Tennessee PSC girder FE simulation results (1) Beam length vs. Vertical stress (2) Beam length vs. Shear stress (3) Beam length vs. Displacement (4) Beam length (Clamping force zone) vs. Displacement.
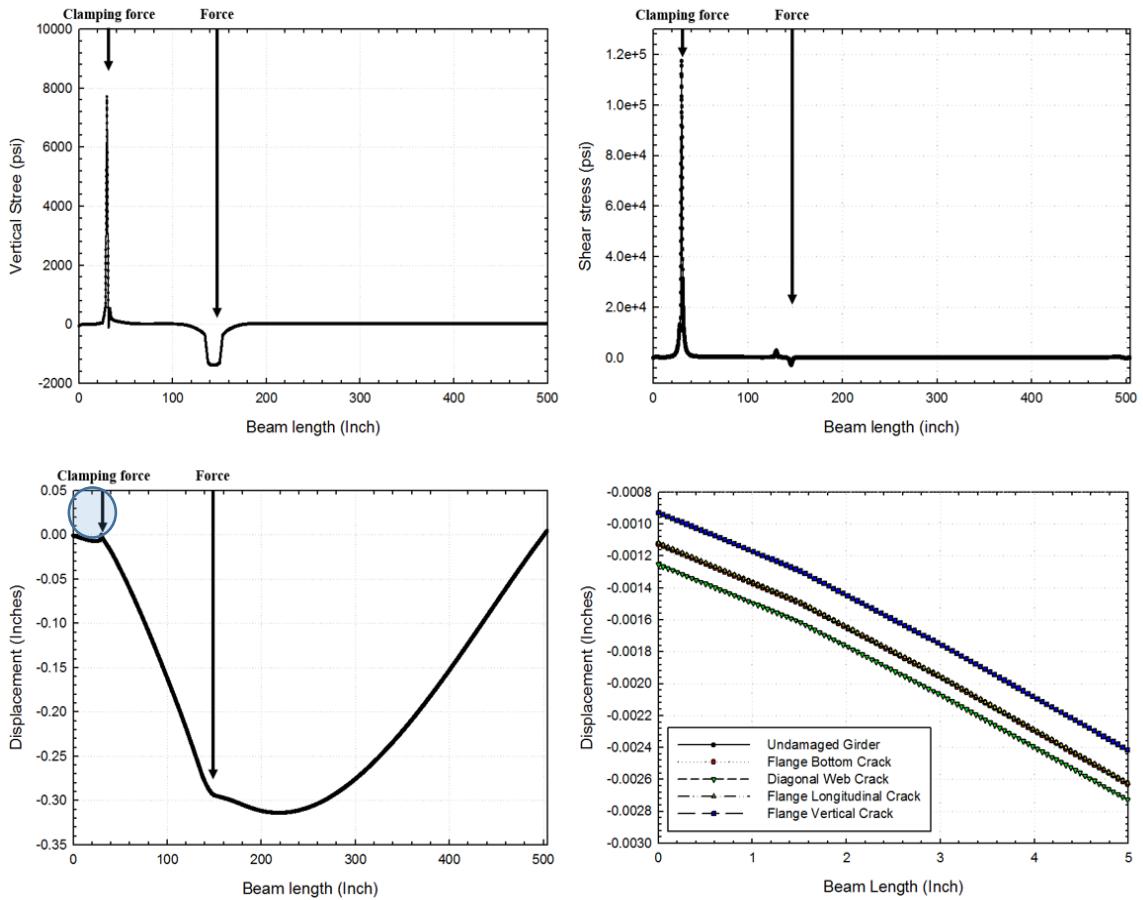
Figure 34: Tennessee PSC girder FE simulation results (1) Beam length vs. Vertical stress (2) Beam length vs. Shear stress (3) Beam length vs. Displacement (4) Beam length (Clamping force zone) vs. Displacement.
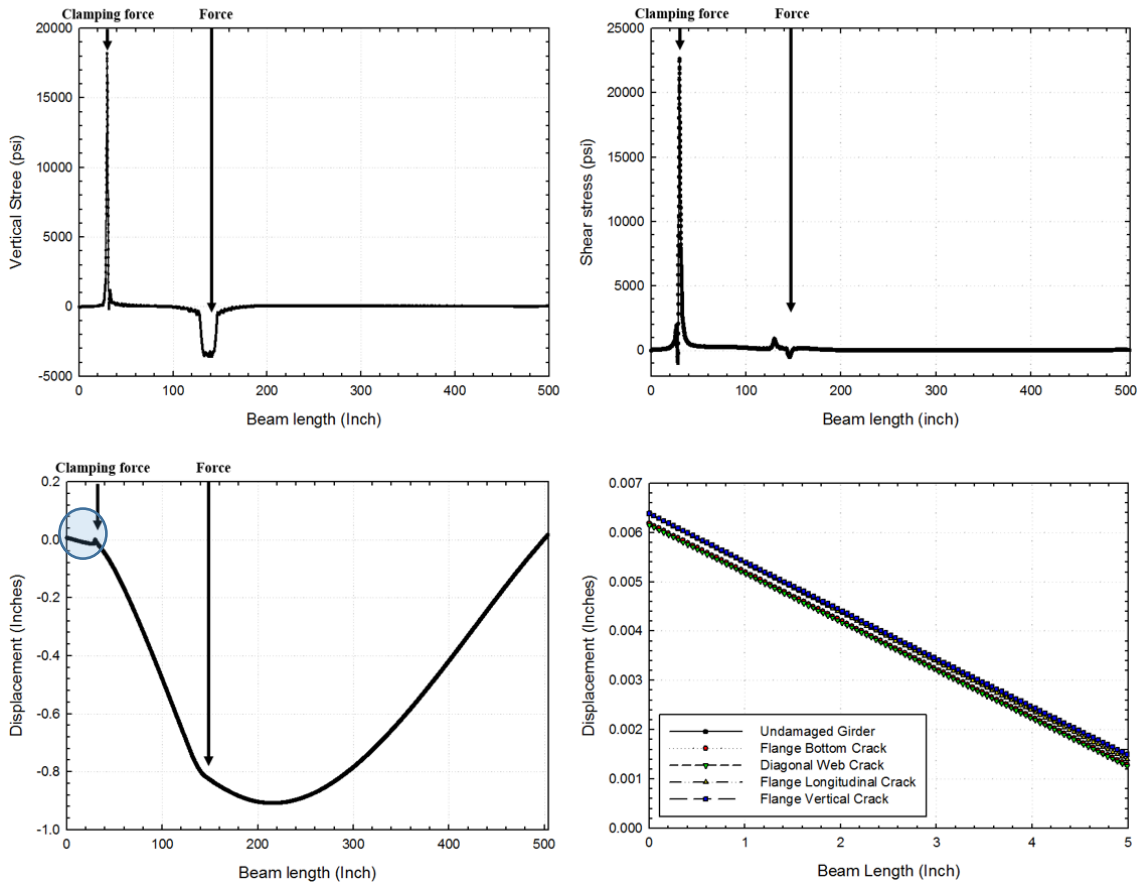
Figure 35: Virginia PSC girder FE simulation results (1) Beam length vs. Vertical stress (2) Beam length vs. Shear stress (3) Beam length vs. Displacement (4) Beam length (Clamping force zone) vs. Displacement.
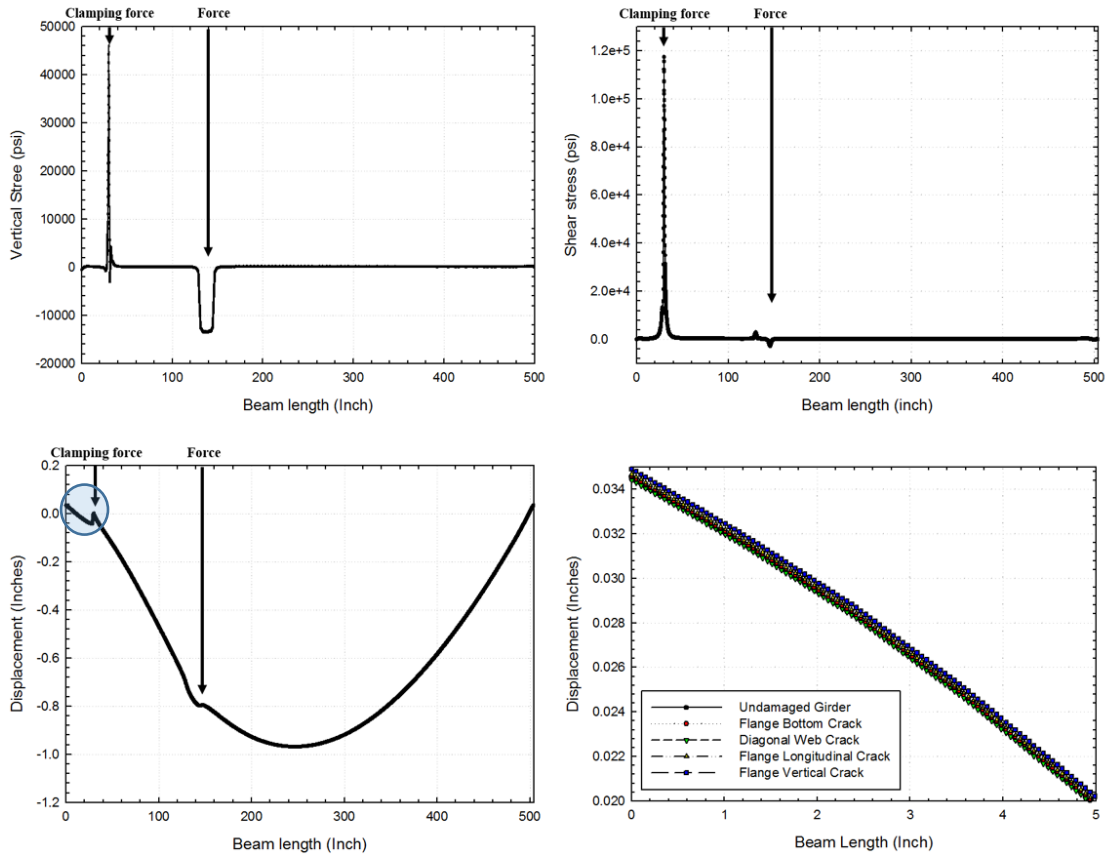
Figure 36: Florida PSC girder FE simulation results (1) Beam length vs. Vertical stress (2) Beam length vs. Shear stress (3) Beam length vs. Displacement (4) Beam length (Clamping force zone) vs. Displacement.

6 COHESIVE ZONE MODELS (CZM)

6.1 BASIC PRINCIPLES OF CZM

As shown in Fig 37 (a), a CZM represents two solid bodies Ω_1 and Ω_2 that have a common boundary S in the initial (reference) configuration. Under specific loading conditions, S_1 and S_2 are separated, as shown in Fig 37 (b). Due to the separation of the boundary S into two boundaries, new internal and external surfaces are created, as shown in Fig 37 (c). This newly created domain Ω_*, surrounded by S_1 and S_2 surfaces, is a 3D domain made of extremely soft glue. In some applications, the domain Ω_* represents a fracture. Fig 37 (d) presents a typical constitutive relationship that can be used to relate traction forces and normal displacements at the faces of the domain Ω_*, in the tip area:

$$\text{If } |\vec{\delta}| < |\vec{\delta}_{sep}|, \qquad \tilde{\sigma}\hat{n} = \bar{T}$$

$$\text{If } |\vec{\delta}| \gg |\vec{\delta}_{sep}|, \qquad \tilde{\sigma}\hat{n} = \bar{T} = 0$$
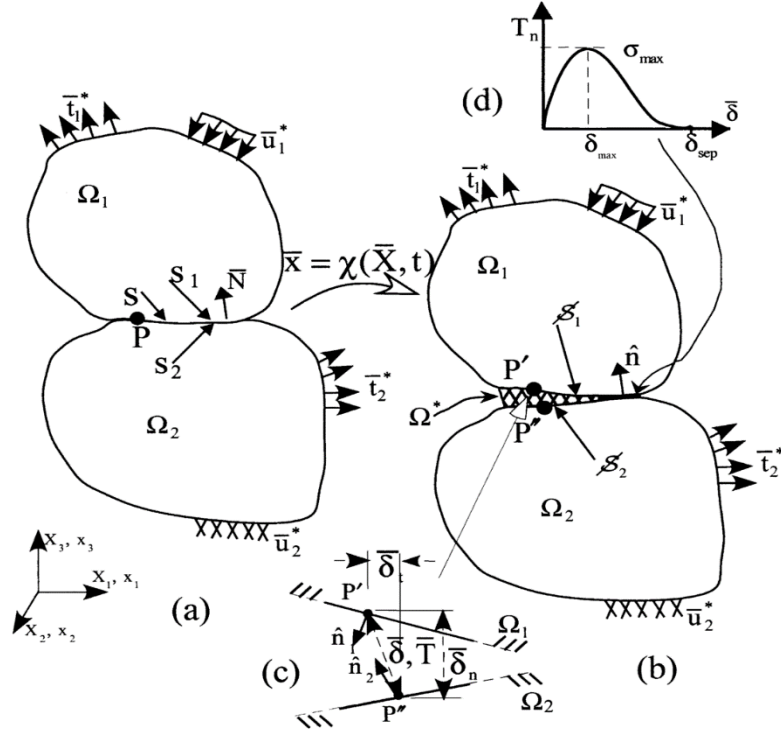
Figure 37: Conceptual framework of Cohesive Zone Models (N. Chandra et al, 2002)

The bilinear model proposed by Geubelle and Baylor in 1998 was employed to predict failure in polycrystalline brittle materials and viscoelastic asphalt concrete. The normal and tangential tractions of the bilinear cohesive traction model are expressed as follows:

$$T_n = \frac{s}{1-s}\overrightarrow{\Delta_n}\sigma_{max}, \quad T_t = \frac{s}{1-s}\overrightarrow{\Delta_t}\tau_{max}$$

Where σ_{max} is the normal cohesive strength, and τ_{max} is the tangential cohesive strength. Internal residual strength variable s is originally assigned an initial value $s_{initial}$ close to unity and vanishes when complete failure is achieved. This strength parameters s defined by:

46

$$s = 1 - \left|\tilde{\Delta}\right|_2 = \min(s_{min}, \text{man}(0, 1 - \left|\tilde{\Delta}\right|_2))$$

$\left|\tilde{\Delta}\right|_2$ denotes the Euclidean norm and $\tilde{\Delta} = (\frac{\Delta_n}{\Delta_{nc}}, \frac{\Delta_t}{\Delta_{tc}})$ denotes the non-dimensionalized displacement jump vector, the components of which are normalized by the critical tensile and shear displacement discontinuities. The displacement jumps Δ_{nc} and Δ_{tc} are expressed as

$$\Delta_{nc} = \frac{2G_{Ic}}{\sigma_{max}s_{initial}}, \quad \Delta_{tc} = \frac{2G_{IIc}}{\tau_{max}s_{initial}}$$

In which G_{Ic} and G_{IIc} are the mode I and II critical energy release rates, respectively.

6.2 CZM APPLICATIONS

Cohesive Zone Models (CZMs) have been widely used to predict the progressive formation of nonlinear fracture process zones in concrete and cementitious composites such as plain concrete, fiber reinforced concrete and asphalt concrete. CZMs are based on traction-separation relationships, such as those presented in Fig 38. Similar relationships are used in mode II. For example, a bilinear CZM model gives a better representation of metal-ceramic interfaces than an exponential CZM model.
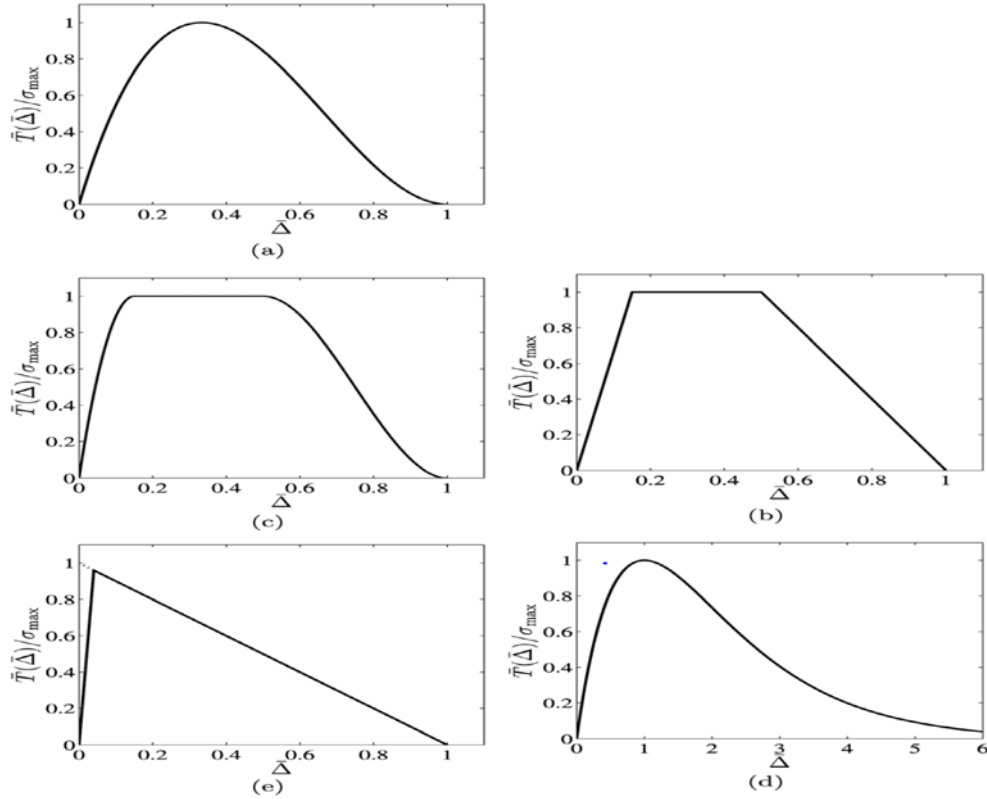
Figure 38: Examples of traction-separation functions: (a) cubic polynomial, (b) trapezoidal, (c) smoothed trapezoidal, (d) exponential, (e) bilinear (K. Park et al., 2010)

For further analysis of girders with end cracks, it is recommended to couple the Continuum Damaged Mechanics model calibrated for concrete (DSID model) with a bilinear CZM, in order to predict the initiation and propagation of cracks over several scales. The approach proved to be successful to simulate the propagation of a meter-scale Mode II discrete fractures in Bakken shale (Fig. 39). The advantage is that the model predicts the geometry of macroscopic cracks and the extent of the damage zone around the tips. The CZM could be easily modified to account for the cohesion of cracks repaired

by epoxy injection. A literature review of epoxy rheological models is provided in the next section.
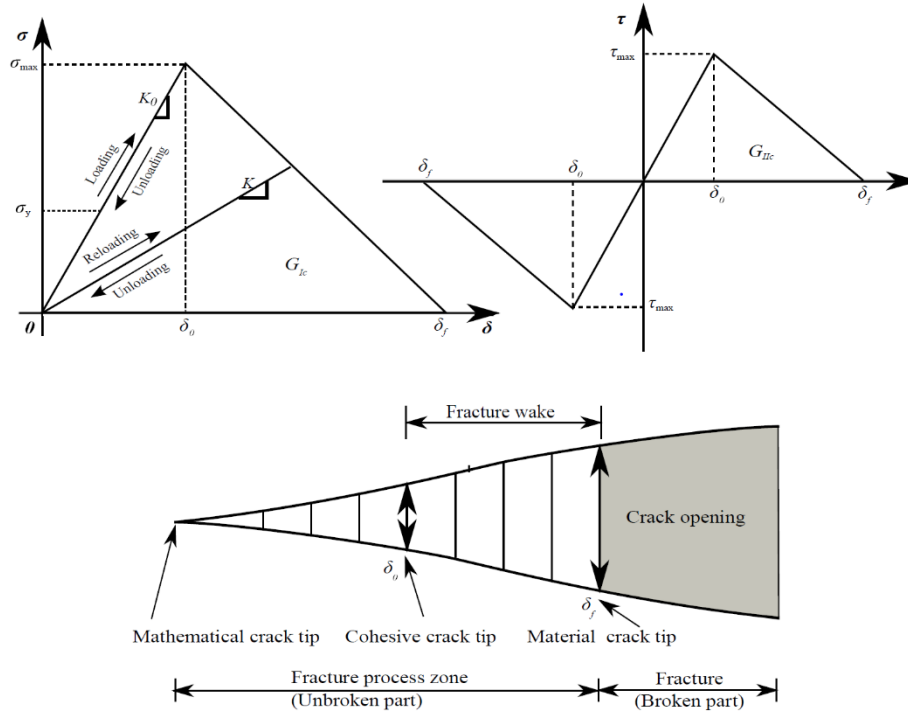
Figure 39: Bilinear Cohesive Zone model (Wencheng Jin et al, 2016)

7. EPOXY RESIN PROPERTIES

7.1 LITERATURE REVIEW

Most epoxy adhesives are employed to connect structural elements made of different materials. In the following, we report the rheological models of epoxy used for sealing applications. Epoxy adhesive properties are summarized in Table 4. Because epoxy adhesives are highly sensitive to thermal conditions, the pot life and bond strength present totally different values at different temperatures.

Table 6: Epoxy adhesive properties (GDOT, 2009, Issa and Debs, 2007, Hong-chol et al., 20017)

Specimen	Pot life (Min)	Bond strength (MPa)	Shelf life (Month)	Thermal coefficient (per $\mathcal{C}$)
G-DOT Recommendation	$10 - 45$ **at 25 $\mathcal{C}$**	2.5	24	-
Hard type Epoxy (Hong-chol)	-	48	-	$\mathbf{3.5 \times 10^{-4}}$
Soft type Epoxy (Hong-chol)	-	3.5	-	$\mathbf{8.0 \times 10^{-3}}$
Epoxy (Issa and Debs)	60 **at 20 $\mathcal{C}$**	4.0	-	$\mathbf{9.0 \times 10^{-5}}$

Hong-chol et al (2011) conducted tension tests to calculate the tensile stress of epoxy hard and soft resins in glassy state (Fig 40). Hard epoxy resin has a high tensile stress at

ambient temperature (25 $\mathcal{C}$), but it cannot undergo more than 8% strains. Soft epoxy resins exhibit opposite trends (low tensile stress, high deformability).
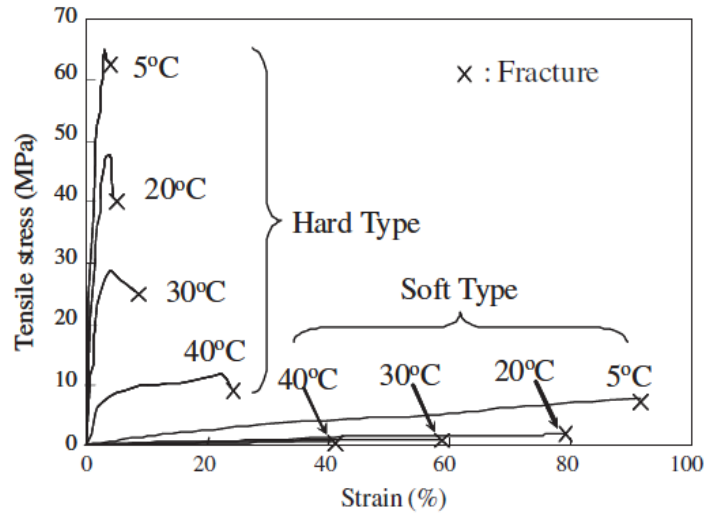
Figure 40: Engineering properties of epoxy resin (Hong-chol Shin et al., 2011)

The viscoelastic behavior of epoxy can be represented by elastic and viscous components modeled as linear combinations of springs and dashpots. The spring represents the potential to store energy, while the dashpot represents the time-dependence of epoxy's behavior:

- Spring, elastic behavior: $\sigma = E\varepsilon$

- Dashpot, viscous behavior: $\sigma = \eta \dfrac{d\varepsilon}{dt}$

Representative models of viscoelasticity are summarized in Fig 41. In Maxwell model, the spring is instantaneously subjected to elastic deformation. Then elastic stress relaxes, the spring is released, which increases the viscoelastic deformation in the dashpot over time. Maxwell model is appropriate for most polymers but it does not predict creep accurately. By contrast, Kelvin-Voigt model is good for modeling creep, but it is less accurate for capturing relaxation. The Standard Linear Solid (SLS) model can be calibrated to capture material responses more accurately than Maxwell and Kelvin-Voigt models. However, the SLS model returns inaccurate results for strain under specific loading conditions. In the following subsection, we explain the rheological model retained to simulate epoxy behavior in this study.
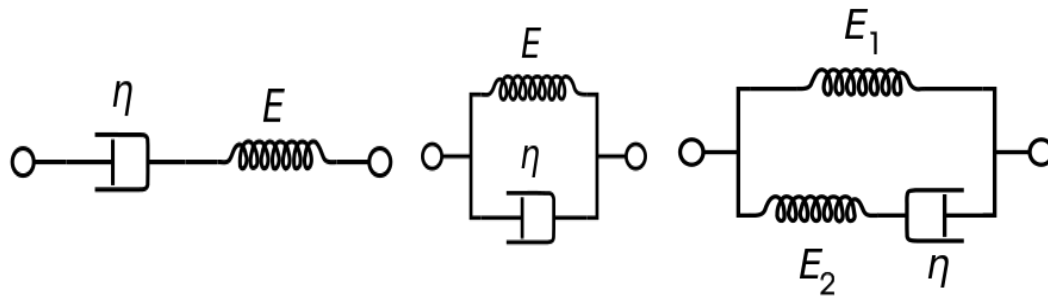
Figure 41: Rheological models of viscoelasticity: Maxwell model (left), Kelvin-Voigt model (center), Standard Linear Solid Model (right). Pictures taken from Wikipedia.

7.2 NONLINEAR VISCOELASTIC BEHAVIOR OF EPOXY RESINS

L. Bardella (2001) conducted creep tests with the epoxy resins and showed that the time-dependent behavior of epoxy is non-linear (Fig 42).
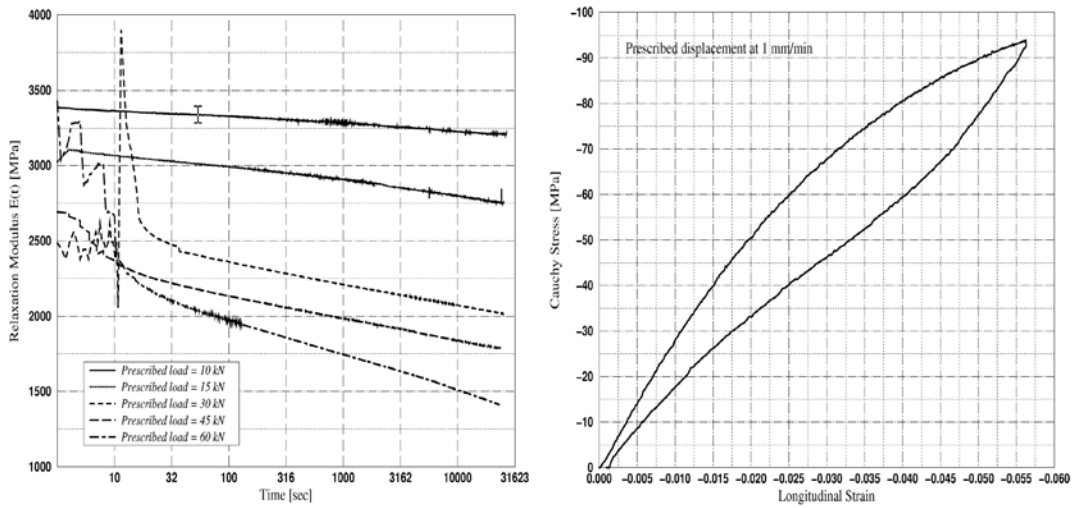
Figure 42: (a) Creep behavior and (b) Cyclic behavior of the epoxy resin DGEBA DER 332 (L. Bardella, 2001)
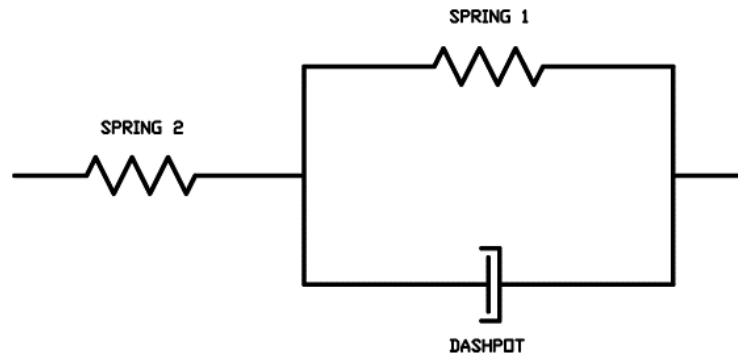
Figure 43: Rheological model for nonlinear viscoelastic behavior of epoxy resins (L. Bardella, 2001)

The constitutive model proposed by L. Bardella (2001) describes the nonlinear viscoelastic behavior of epoxy resins in the glassy state. The angular frequency of molecular jumps between two rotational isomeric states can be obtained by Arrhenius equation, as follows:

$$\omega = \omega_0 \exp \frac{-\Delta G_s}{k_B T}$$

$$\omega_0 = 2\pi \frac{k_B T}{h_P}$$

Where G_s and k_B are the Gibbs free energy and the Boltzmann constant. h_P is the Planck constant. Based on the Eyring theory (Eyring, 1936), the net molecular flow in the forward direction is:

$$\omega_{net} = \omega_f - \omega_b = \omega_0 \exp \frac{-\Delta G_s}{k_B T} \sinh \frac{\sigma \upsilon}{k_B T}$$

In which υ is the activation volume associated with the uniaxial stress σ. Considering the fundamental hypothesis in deriving the Eyring model, the new flow ω_{net} and $\dot{\varepsilon}_{net}$ are related by the dimensionless constant ($\dot{\varepsilon}_0 = \in \omega_0$). The Eyring model can be expressed in terms of the $\dot{\varepsilon}_{net}$:

$$\dot{\varepsilon}_{net} = \dot{\varepsilon}_0 \exp \frac{-\Delta G_s}{k_B T} \sinh \frac{\sigma_{eq} \upsilon}{k_B T}$$

Because we consider three-dimensional stress states, the equivalent strain rate $\dot{\varepsilon}_{eq}$ can be related to the equivalent stress σ_{eq}:

$$\dot{\varepsilon}_{eq} = \sqrt{\frac{2}{3} \dot{\varepsilon}_{ij} \dot{\varepsilon}_{ij}}$$

$$\sigma_{eq} = \sqrt{\frac{2}{3} s_{ij} s_{ij}}$$

Ramberg-Osgood constitutive law allows simulating the nonlinear behavior of epoxy resins. The rheological model, illustrated in Fig.43, links the deviatoric stresses and strains acting on spring 1, as follows:

$$s_{ij}^{(1)} = \frac{2G_1}{1 + \alpha(\frac{\sigma_{eq}^{(1)}}{\sigma_0})^{n-1}} e_{ij}^{(\upsilon)}$$

Where G_1, α, σ_0, and n are material constants and $e_{ij}^{(\upsilon)}$ is the viscoelastic strain present both in the spring 1 and in the dashpot. The stress $\sigma_{eq}^{(v)}$ can be expressed based on Eyring model:

$$\sigma_{eq}^{(v)} = \frac{k_B T}{\upsilon} \mathrm{arcsin}\, h(\frac{\dot{\varepsilon}_{eq}^{(\upsilon)}}{\dot{\varepsilon}_0} \exp \frac{\Delta G_s}{k_B T})$$

A tensorial stress-strain relationship is obtained to model the dashpot behavior:

$$s_{ij}^{(\upsilon)} = \frac{2\dot{e}_{ij}^{(\upsilon)}}{3\dot{\varepsilon}_{eq}^{(\upsilon)}} \sigma_{eq}^{(\upsilon)}$$

Based on the above equations, the constitutive relation can be derived:

$$s_{ij} = \frac{2G_1}{1 + \alpha(\frac{\sigma_{eq}^{(1)}}{\sigma_0})^{n-1}} e_{ij}^{(\upsilon)} + \frac{2\dot{e}_{ij}^{(\upsilon)}}{3\dot{\varepsilon}_{eq}^{(\upsilon)}} \frac{k_B T}{\upsilon} \mathrm{arcsin}\, h(\frac{\dot{\varepsilon}_{eq}^{(\upsilon)}}{\dot{\varepsilon}_0} \exp \frac{\Delta G_s}{k_B T})$$

In which

$$e_{ij}^{(v)} = e_{ij} - \frac{s_{ij}}{2G_2}$$

$$\dot{e}_{ij}^{(v)} = \dot{e}_{ij} - \frac{\dot{s}_{ij}}{2G_2}$$

And $\sigma_{eq}^{(1)}$ can be computed by means of the implicit relation:

$$\sigma_{eq}^{(1)} = \frac{3G_1}{1 + \alpha(\frac{\sigma_{eq}^{(1)}}{\sigma_0})^{n-1}} \varepsilon_{eq}^{(v)}$$

$$\varepsilon_{eq}^{(v)} = \sqrt{\frac{2}{3} e_{ij}^{(v)} e_{ij}^{(v)}}$$

The non-linear viscoelastic constitutive law proposed for epoxy resins in glassy state can be implemented in ABAQUS Finite Elements or Cohesive Zones to simulate repaired concrete by epoxy resins.

8. CONCLUSIONS & RECOMMENDATIONS

8.1 CONCLUSIONS

The ultimate goal of this project is to assess the mechanical integrity and sustainability of pre-stressed concrete beams during the entire life cycle of the built infrastructure, which includes crack propagation, crack reparation, repaired crack aging with possible re-opening. In Phase I, the research objectives are to: (1) Explain in which conditions the strength of cracked concrete can be recovered by epoxy injection; (2) Design the injection method for optimal mechanical performance. The progress made to meet these objectives is summarized below.

(1) Explain in which conditions the strength of cracked concrete can be recovered by epoxy injection.

Task 1.1. Literature review: thermo-hydro-mechanical properties of epoxy and other polymers used for concrete reparation

We studied the laboratory tests performed to characterize the thermo-elastic and creep properties of epoxy. We summarized epoxy constitutive laws and parameters reported in the literature. We also explained how epoxy is used to repair cracked concrete. We gathered reference experimental datasets on the stiffness and strength properties of concrete that contains no crack (undamaged concrete), that contains open cracks (damaged concrete), and that contains cracks partially or totally filled with

57

epoxy (repaired concrete). We also collected technical literature on the design of pre-stressed concrete beams for typical bridge girders.

Task 1.2. Theoretical modeling: Continuum Damage Mechanics (CDM) model (DR1) including the effects of crack propagation before and after epoxy injection

We presented the governing equations of the Differential Stress-Induced Damage model (DSID), a Continuum Damage Mechanics model that allows predicting the propagation of cracks in three directions, according to net tension and compression criteria. The damage variable is similar to a crack density tensor. For example, horizontal damage is related to the volumetric fraction of cracks contained in plane normal to the horizontal, i.e. vertical cracks. Simulations can be used to calculate the stresses and strains in concrete before and after epoxy injection (with high or low damage, respectively).

Task 1.3. Simulations: validation, calibration and sensitivity analysis of model DR1 based on stress paths typical of laboratory tests, for intact, cracked and repaired concrete

We calibrated and validated the DSID model to match stress/strain curves obtained during concrete triaxial compression tests reported in the literature. We performed sensitivity analyses of the DSID model with a MATLAB code. Simulations were done at the material point for tensile and compressive stress paths. Results show that cracks propagate in planes

perpendicular to the maximum deviatoric stress, and that stiffness decreases in the directions in which damage increases. Simulations confirm that mechanical effects of cracks before and after reparation can be modeled by high and low damage. However, further calibration is needed to find an equivalence between the phenomenological damage variable used in the model and actual crack densities.

(2) Design the injection method for optimal mechanical performance

Task 2.1. Simulations: sensitivity analysis of model DR1 to crack orientation, crack density, level of crack density at which epoxy is injected, crack volume fraction filled by epoxy during injection

We designed a Finite Element model of bridge deck with ABAQUS software. The model includes the steel-reinforced concrete deck and the pre-stressed steel-reinforced girders. We applied the static loads recommended in the design standards to predict the displacement and stress fields in the structure. Concrete was first considered elastic. Simulation results highlight the high stress concentrations at the ends of the girders and at the contact between the girders and the rubber pads lying at the top of the supporting columns. Then the FEM model was modified to account for crack propagation in the concrete. Elastic concrete elements located in the girder subject to maximal stress (further away from the center of the deck) were replaced by damageable elements. The DSID model was used to predict damage in the concrete. DSID parameters

calibrated in Task 1.2 were used. Static service loads were simulated. Results highlight the capability of the model to predict the initiation and orientation of the damage in the form of vertical cracks close to the interface between the concrete and the rubber pads. Bridge simulations were repeated with initial damage in the end zone of the most highly stressed girder in the deck. Damage configurations corresponded to typical crack patterns listed in the PCI bridge repair guidelines. In general, lower stress and higher deflections were predicted for higher initial damage.

Task 2.2. Analysis: hand computations with the DR1 model to compare the theoretical deflection of an intact, cracked and repaired girder and assess the validity of the NCHRP recommendations for bridge reparation (based on crack width)

Due to the complexity of the cross-section of the steel-reinforced concrete girders, we used the Finite Element Method instead of hand calculations to predict the deflection of four girders used in Tennessee, Washington State, Virginia and Florida. We simulated a load tests performed on full-scale girders by other authors, with and without initial damage. Initial damage values were chosen so as to represent four typical crack patterns described in the PCI manual, including: vertical cracks, horizontal cracks, diagonal cracks and cracks on the bottom flange. Simulation results did not indicate any significant impact of initial damage on stress distributions for the tests simulated. The effect of initial cracks on deflection was minimal; increased displacements were only noted in the area close to the point of

application of the clamping force. The most noticeable effects on deflection were obtained for vertical and diagonal cracks. The simulation results show that smeared damage in the end zone does not affect the mechanical response of the girder during the vertical load test. Note that epoxy reparation could still be used to prevent steel corrosion (not studied in this project). The continuum is only suitable to represent distributions of non-interacting microscopic cracks. In practice, pre-stressed steel bar relaxation can cause the formation and propagation of cracks with a length of the same order of magnitude of the height of the girder. The formation of a macroscopic crack is the result of micro-crack interaction and coalescence. These phenomena cannot be accounted for in the continuum damage mechanics model that we employed in Phase I of this project, which is only suitable of dilute crack distributions. Further analyses are therefore needed to calibrate the phenomenological damage variable against actual crack densities. In addition, the analyses presented in this report are solely based on the simulation of static loading tests performed on isolated beams, because experimental data was available to compare numerical predictions to actual physical measurements. More simulations and parametric studies are needed to check the response of girders under a variety of stress paths including cyclic loading.

Task 2.3. Synthesis: recommendations of loading and reparation cycles for optimal flexion and shear strength, based on the parametric studies and on the deflection analysis

In order to confirm that cracks induced by static loads do not need structural reparation and to predict the geometry of cracks and not only their average effect on stiffness, we will use a Cohesive Zone Model (CZM) to represent crack patterns in the end zone. We presented a literature review of CZM, which can be used instead of the DSID model, or can be coupled to the DSID model to predict the simultaneous propagation of cracks and their damage zone around the tip. The CZM provides an explicit geometric representation of cracks, which allow determining the range of crack orientations that need to be considered for potential injection, the critical density of cracks in this range of orientations at which injection is needed, the fraction of crack volume that needs to be filled with epoxy. We will examine several design criteria, including allowable girder deflection, allowable concrete stresses and strains, and optimal concrete strength in compression and shear. We will check whether PCI reparation recommendations are conservative or not.

8.2 RECOMMENDATIONS FOR FUTURE WORK

The objective of Phase II of this project is to predict concrete mechanical recovery by epoxy injection, in order to check the girder acceptance criteria recommended by the NCHRP and by the PCI.

Task 1: Numerical prediction of the mechanical performance of damaged concrete before and after epoxy injection.

We will predict the mechanical behavior of cracked concrete before and after epoxy injection with the FEM. In order to better understand the mechanical influence of large cracks formed by micro-crack coalescence, we envision calibrating the phenomenological damage variable against actual crack densities and use a CZM instead of or coupled with the DSID model. Published mechanical tests performed on cracked concrete samples will be used for model calibration and validation. By contrast with the work presented in Phase I, which focused on one loading test performed on several types of girders, we will simulate several stress paths, in particular the typical static and dynamic service loads. By covering a broader range of damage propagation scenarios during steel reinforcement relaxation and during service loading, we will be able to identify the crack patterns that are detrimental to the mechanical integrity of the girders. Then, we will modify the CZM concrete model to account for the presence of epoxy filling the cracks. We will model of adhesion recovery as a function of crack filling and epoxy properties – which depend on temperature and time. Experimental data published in the literature will be used for calibration. Sensitivity analyses will be conducted to assess the mechanical integrity of pre-stressed bridge girders for a variety of crack and injection patterns.

Task 2: Assessment of NCHRP and PCI recommendations.

The NCHRP recommends to (Tadros et al., 2010): Accept the girders if longitudinal cracks are less than 0.012 in. wide; Apply cementitious packing materials to cracks between 0.012 in. and 0.025 in. wide; Inject epoxy in cracks that are 0.025 in. to 0.050 in. wide; reject the girder (and replace it) if cracks are wider than 0.05 in. The PCI (2001) also uses three defect categories (those that can be accepted without repair, those that can

be repaired, those that must be rejected), but has more detailed trouble shooting and reparation procedures, depending on the location, orientation, length and width of the cracks. We will implement the numerical model proposed in Task 1 to simulate the evolution of stress, deformation and damage in servicing girders, with and without pre-stress cracks, and with and without epoxy injection. We will examine individually each of the standard repair procedures described by the NCHRP and by the PCI. We will identify the cracks that are structurally critical, and we will define a damage index to recommend girder acceptance, reparation or rejection according to a variety of servicing scenarios (including girder geometry, loading, temperature, materials….) The final product this Phase II research will be a copy of standard beam repair procedures that will help GDOT's engineers and inspectors deciding whether defects observed on girders can be accepted, and if not, whether they can be repaired, and how. We will also simulate the life cycle of pre-stressed girders under typical loading conditions.

9. REFERENCES

1. Akira Tasat, 1988. Resistance of Flexural Reinforced Concrete Members after Repair with Epoxy Resin. *9th World Conference on Earthquake Engineering*

2. Amar Prakash, N. Anandavalli, C. K. Madheswaran, J. Rajasankar, N. Lakshmanan. 2011. Three dimensional FE Model of Stud Connected Steel-Concrete Composite Girders Subjected to Monotonic Loading, *International Journal of Mechanics and applications*. 1(1). pp. 1-11.

3. Arson, C. (2014). Generalized Stress Variables in Continuum Damage Mechanics, Mechanics Research Communications, DOI: 10.1016/j.mechrescom.2014.06.006

4. B. G. Rabbat, H. G. Russell, 1985. Friction Coefficient of Steel on Concrete or Grout. *Journal of Structual Engineering,* 111(3), pp. 505-515.

5. By D. C. Candappa, J. G. Sanjayan, and S.Setunge, 2001. Complete Triaxial Stress-Strain Curves of High-Strength Concrete. *Journal of Materials in Civil Engineering,* 13(3), pp. 209-215.

6. Calvin E. Reed, Robert J. Peterman, Hayder A. Rasheed, 2005. Evaluating FRP reparing method for Cracked Prestresed Concrete Bridge Members Subjected to Repaired Loadings Phase1.

7. Camille A. Issa, Pauls Debs, 2007. Experimental study of epoxy repairing of cracks in concrete. *Construction and Building Materials*, *21*, 157-163.

8. Can Akogul, Oguz C. Celik, 2008. Effect of Elastomeric Bearing Modeling Parameters on The Seismis Design of RC Highway Bridges with Precast Concrete Girders, *The 14ᵗʰ World Conference on Earthquake Engineering.*

9. D.W. Fowler, 1999. Polymers in concrete: a vision ofr the 21ˢᵗ century. *Cement & Concrete Composites,* pp. 449-452.

10. Dongming Wei, Mohamed B. M. Elgindi, 2013. Finite Element Analysis of the Ramberg-Osgood Bar. *American Journal of Computational Mathematics,* pp. 211-216.

11. Dry, C., Corsaw, M., & Bayer, E. (2003). A comparison of internal self-repair with resin injection in repair of concrete. *Journal of adhesion science and technology*, *17*(1), 79-89.

12. Georgia Department of Transportation, 2016. Bridge and Structures Design Manual

13. Geubelle and Baylor. Impact-induced delamination of composites: a 2D simulation, Composites Part B 29B (1998) 589-602.

14. Hao Xu, Chloe Arson, 2014. Anisotropic Damage Models for Geomaterials: Theoretical and Numerical Challenges. *International Journal of Computational Methods*, Special Issue on Computational Geomechanics, vol.11, n.2, DOI: 10.1142/S0219876213420073

15. Hao Xu, Chloe Arson., 2015. Mechanistic Analysis of Rock Damage Anisotropy and Rotation Around Circular Cavities. *Rock Mechanics Rock Engineering*, DOI 10.1007/s00603-014-0707-5

16. I. A. Basunbul, A. A. Gubati, G. J. Al-Sulaimani, and M. H. Baluch, 1990. *ACI Materials Journal,* pp. 348-354.

17. I. Imran, S. J. Pantazopoulou, 1996. Experimental Study of Plain Concrete under Triaxial Stress*, ACI Materials Journal*. pp. 589-601

18. Jeffrey Roesler et al. Concrete fracture prediction using bilinear softening, *Cement & Concrete Composites*. 29 (4) (2007) 300-312.

19. K. Park et al. Cohesive zone model for functionally graded fiber reinforced concrete, *Cement & Concrete Composites*. 40 (6) (2010) 956-965.

20. Kunieda Minoru, Kamada Toshiro, Uchida Yuichi, and Rokugo Keitetsu., 2001. Evaluation of Bond Properties in Concrete Repair Materials. *Journal of Materials in Civil Engineering,* 13(2), pp. 98-105.

21. Lorenzo Bardella., 2001. A phenomenological constitutive law for the nonlinear viscoelastic behavior of epoxy resins in the glassy state. *Construction and Building Materials*, *21*(1), 157-163.

22. M. Elices et al. The cohesive zone model: advantages, limitations and challenges, *Engineering Fracture Mechanics* 69 (2002) 137-163.

23. Modjeski and Masters, Inc., 2003. COMPREHENSIVE DESIGN EXAMPLE FOR PRESTRESSED CONCRETE (PSC) GIRDER SUPERSTRUCTURE BRIDGE WITH COMMENTARY. *NRC Research Press* pp. 222-230.

24. N. Chandra et al. Some issues in the application of cohesive zone models for metal-ceramic interfaces, *International Journal of Solids and Structures* 39 (2002) 2827-2855.

25. P. Duarte, J.R. Correia, J.G. Ferreira, F. Numes, and M.R.T. Arruda, 2014. Experimental and numerical study on the effect of repairing reinforced concrete cracked beams strengthened with carbon fiber reinforced polymer laminates. *Administrative Science Quarterly, 44,* pp. 82-111.

26. Petr Bernardin, Josef Vacik, Tomas Kroupa, Radek Kottner., 2013. Determination of The Mechanical Parameters of a Bonded Join Between a Metal and a Composite by Comparing Experiments with a Finite-Element Model. *Materials and technology,* 47(4), pp. 417-421.

27. Precast/Prestressed Concrete Institute (PCI), 2012. *Bridge Member Repair Guidelines.* Report PCINER-01-BMRG

28. S. H. Song et al. Simulation of crack propagation in asphalt concrete suing an intrinsic cohesive zone model, J. Eng. Mech. – ASCE 132 (11) (2006) 1215-1223.

29. Shin, H. C., Miyauchi, H., & Tanaka, K., 2011. An experimental study of fatigue resistance in epoxy injection for cracked mortar and concrete considering the temperature effect. *Construction and Building Materials*, *25*(3), 1316-1324.

30. Tadros, M. K., Badie, S. S., & Tuan, C. Y, 2007. Evaluation and Repair Procedures for Precast/Prestressed Concrete Girders with Longitudinal Cracking in the Web, *654*, Transportation Research Board.

31. Vassilis K. Papanikolaou, Andreas J. Kappos, 2007. Confinement-sensitive plasticity constitutive model for concrete in triaxial compression. *International Journal of Solids and Structures,* 44, pp. 7021-7048.

32. Wencheng Jin, Hao Xu and Chloé Arson. Computational Model Coupling Mode II Discrete Fracture Propagation with Continuum Damage Zone Evolution, *International Journal For Numerical And Analytical Methods In Geomechanics*, 200; 00:1-6

33. Yong-Rak Kim et al. Damage-induced modeling of asphalt mixtures through computational micromechanics and cohesive zone fracture, *Journal of Materials in Civil Engineering*. 17 (5) (2005) 477-484.

34. Yuqing Zhang et al., 2016. Weak Form Equation Based Finite Element Modeling of Viscoelastic Asphalt Mixtures. *Journal of Materials in Civil Engineering,* 28(2), pp. 417-421.